EA-6010-12
(Formerly FE-3800)
Dist. Category UC-90C

MATERIALS RESEARCH FOR CLEAN UTILIZATION OF COAL

QUARTERLY PROGRESS REPORT

April – June 1977

Samuel J. Schneider
Program Manager

Institute for Materials Research
National Bureau of Standards
Washington, D. C. 20234

PREPARED FOR THE UNITED STATES
ENERGY RESEARCH AND DEVELOPMENT ADMINISTRATION

Under Contract No. EA-77-A-01-6010
(Formerly E(49-1)-3800)

TABLE OF CONTENTS

I. OBJECTIVE AND SCOPE OF WORK

Coal Gasification processes require the handling and containment of corrosive gases and liquids at high temperature and pressures, and also the handling of flowing coal particles in this environment. These severe environments cause materials failures which inhibit successful and long-time operation of the gasification systems. The project entails investigations on the wear, corrosion, chemical degradation, fracture, and deformation processes which lead to the breakdown of metals and ceramics currently being utilized in pilot plants. Studies will also be carried out on new candidate materials considered for improved performance. Special emphasis will be devoted to the development of test methods, especially short-time procedures, to evaluate the durability of materials in the gasification environments. These methods will focus on wear, impact erosion, stress corrosion, strength, deformation, a slow crack growth and chemical degradation of refractories. A system has been initiated to abstract and compile all significant operating incidents from coal conversion plants. This program will provide a central information center where problems of common interest can be identified and analyzed to avoid unnecessary failures and lead to the selection of improved materials for coal conversion and utilization. Active consultation to ERDA and associated contractors will be provided as requested.

II. SUMMARY OF PROGRESS TO DATE

Brief Summary

1. Metal Corrosion

a. Constant Strain-Rate Test

The set-up and calibration of gas mixing apparatus was completed for testing in coal gasification environments except for supplying steam since a failure occurred in the feed pump to the steam generator. The original schedule for testing the alloys was modified to do the normalizing environment (e.g., helium) first instead of the oxidizing environment. The testing of all scheduled alloys at $10^{-6}s^{-1}$ at 450 °C (840 °F) and 600 °C (1100 °F) in ultra-pure helium was completed. When testing Inconel 671 at 600 °C (1100 °F), a very significant decrease in properties (tensile strength, elongation, and reduction in area) occurred when compared to the results obtained when Inconel 671 was tested at 450 °C (840 °F). This brittle type failure was similar to what had previously been reported for 310SS. The brittle type failure in Inconel 671 was attributed to the formation of the brittle alpha chromium phase formed at 600 °C (1100 °F).

The above mentioned brittle failure of Inconel 671 and the previously reported brittle failure of stainless steel type 310 indicate the possibility of premature brittle failure of stressed components manufactured of these alloys when used at elevated temperatures-- apparently, regardless of the environment to which they are exposed.

1

b. Pre-Cracked Fracture Test

Elastic stress analyses were done to evaluate various modifications to
the wedge loaded DCB specimen to account for changes in elastic
modulus and thermal expansion. Additional modifications are being
considered to the specimen to reduce the effect of temperature on the
stress-intensity factor.

2. Ceramic Deformation, Fracture and Erosion

Work is continuing on construction and assembly of a high-temperature,
high-pressure mechanical loader. A three zone furnace assembly has been
constructed around the inner environmental chamber, and is being charae-
terized as a function of temperature and pressure. As part of the
mechanical testing of refractory concretes after exposure, a study has
been initiated in a 70% H_2O - 30% CO_2 environment. Preliminary data
on a high-alumina concrete exposed at 610°C showed a slight increase
in strength at room temperature. The formation of calcium carbonate
was also observed.

3. Chemical Degradation

a. Reactions and Transformations

Construction of the pressure vessel for x-ray diffraction measure-
ments has been completed. External heaters and safety shields have
been installed, and calibration runs with a saturated steam atmosphere
are in progress. Tests to date show that additional insulation will
be needed to permit operation at 1000°C without overheating the outer
wall of the pressure vessel. Meanwhile, five additional standard
patterns have been prepared. In situ diffraction measurements are
expected to begin during August.

b. Slag Characterization

A pressure vessel for the determination of the viscosity of molten
slag compositions in steam has been designed, constructed and
preliminary heatings made at ambient pressure. The system has a
design capability of 300 psig and 1450°C.

c. Vaporization and Chemical Transport

Calibration tests and vapor transport measurements on relatively
simple coal impurity systems (Na_2SO_4 and NaCl) were made during the
third quarter. The technique and results were reported on by
Dr. Bonnel at the Twenty Fifth Conference on Mass Spectrometry and
Allied Topics (Washington, D.C.). A copy of the extended abstract
for this paper is included as an appendix to this report. These
data indicated a very satisfactory performance by the reactor for
gas pressures up to 1 atm and temperatures of up to about 1400°C.
Species partial pressure measurements over a wide range of temperature
and pressure are planned for more complex systems involving compounds
comprised of Na, S, Cl, O, and H.

2

4. Failure Prevention

The Failure Prevention Information Center continued to expand its data collection activity. Fifty-eight additional reports of operating experiences and failure analysis were received, classified, evaluated and entered into the data base. Additional statistical programs were developed and modified for analyzing and outputing these data. Direct contact with plant managers and engineers was initiated and a detailed plan for conducting the first post inactivation analysis of an operating pilot plant was written.

Articles Published and Talks Presented

G. Ugiansky chaired the ASTM/NACE Symposium on "Constant Strain-Rate Testing" and presented a paper, "Constant Strain-Rate Stress Corrosion Testing of Metals in Gaseous Environments at Elevated Temperatures."

Dr. Bonnel presented a paper entitled, "Transpiration Mass Spectrometry Studies of the Thermal Decomposition and Sublimation of Sodium Sulfate," at the Twenty Fifth Annual Conference on Mass Spectrometry and Allied Topics (Washington, D.C., May 29-June 3, 1977).

J. M. Bukowski, E. R. Fuller, Jr., and C. R. Robbins, "Microstructural and Mechanical Properties of Calcium Aluminate Refractories after High Temperature Pressure Exposure," American Ceramic Society, 79th Annual Meeting, April 27, 1977, Chicago, Illinois.

S. M. Wiederhorn and D. E. Roberts, "Erosion of Castable Refractories for Coal Gasification Applications," American Ceramic Society, 79th Annual Meeting, April 27, 1977, Chicago, Illinois.

III. DETAILED DESCRIPTION OF TECHNICAL PROGRESS

1. Metal Corrosion

a. Constant Strain-Rate Test (G. M. Ugiansky and C. E. Johnson, 312.04)

Progress: The set-up for testing alloys in coal gasification
environments was completed. A preliminary test run at 600°C (1100°F)
at a strain rate of 10^{-6} s^{-1} with 310S and 347 SS specimens was used
to check out the system. A failure in the pump supplying distilled
water to the steam generator prevented the test from continuing in
the oxidizing coal gasification environment. The 310S and 347 SS
specimens were allowed to run in a dry atmosphere of 99% gas mixture
(23.8% CO, 31.8% CO_2, 23.1% H_2, 21.3% CH_4) and 1% H_2S. The results
of the preliminary test run at 600°C (1100°F) at a strain rate of 10^{-6}
s^{-1} in that dry atmosphere show that the elongation and reduction in
area for 310S and 347 stainless steel were virtually the same as for
310S and 347 SS tested at 540°C (1000°F) in H_2S which had been
saturated with water vapor at room temperature.

The original schedule for testing the various alloys in coal
gasification environments called for set up and calibration of gas
mixing apparatus (milestone 1a-1), tests in an oxidizing environment
(milestone 1a-2), a normalizing environment (milestone 1a-3), and a
reducing environment (milestone 1a-4). With the failure in the
pumping system and in the conservation of time, the schedule of tests
was changed and the tests in the normalizing environment were run
first. These tests have been completed for the various alloys at two
test temperatures, 450°C (840°F) and 600°C (1100°F), at a strain rate
of 1 X 10^{-6} s^{-1} in ultra-pure helium. The data tabulated in table 1
are for the various alloys tested at 450°C (840°F). Of these alloys
only 310 SS had previously been tested at or near this temperature.
It should also be noted that there is data for two new alloys not
previously tested, 446 SS (ferritic) and Inconel 671 (50 nickel 50
chromium).

Table 1

Alloy Tests at 450°C (840°F) at 1 X 10^{-6} s^{-1} in Ultra-Pure Helium

| Alloy | Tensile Strength | | Elongation | RA |
	MPa,	psi	%	%
310 SS	602	87,300	37.9	64.6
310S SS	518	75,100	38.9	63.7
347 SS	568	82,300	18.8	65.2
446 SS	587	85,000	17.3	57.0
In 800	526	76,200	37.3	72.1
In 671	680	98,600	32.8	37.7

Table 2 shows the data for the various alloys tested at 600°C (1100°F).

Table 2

Alloy Tests at 600°C (1100°F) at 1 X 10^{-6} s^{-1} in Ultra-Pure Helium

Alloy	Tensile Strength		Elongation %	RA %
	MPa,	psi		
310 SS	415	60,100 (−31%)*	19.9 (−47%)	28.8 (−55%)
310S SS	437	63,400 (−16%)	31.9 (−18%)	42.8 (−33%)
347 SS	451	65,300 (−21%)	13.4 (−29%)	52.2 (−20%)
446 SS	152	22,000 (−74%)	62.0 (+358%)	86.2 (+151%)
In 800	467	67,700 (−11%)	37.1 (−0.5%)	60.1 (−17%)
In 671	425	61,600 (−37%)	13.3 (−59%)	15.6 (−59%)
In 671 (2nd Run)	416	60,300 (−39%)	16.1 (−51%)	16.3 (−57%)

*Note: The percent numbers in parentheses in table 2 show the effect of increase in test temperature from 450°C (840°F) to 600°C (1100°F) whether the values of the properties decrease or increase when compared to data in table 1.

It was previously known that the increase in temperature caused a significant decrease in property values for 310 SS due to a brittle type fracture. The 310S was less affected by the temperature increase than was 310 SS. The 347 SS also showed a decrease in property values due to the temperature increase. Although Incoloy 800 showed a decrease in property values, it was the least affected by the temperature increase. One of the new alloys tested, ferritic 446 SS, showed a large decrease in tensile strength when tested at 600°C (1100°F) as compared to the tensile strength when tested at 450°C (840°F). This large decrease was due to softening of the metal; the 600°C (1100°F) temperature was above the temperature at which 446 SS would be used. The large increase in elongation and reduction in area was also due to the softening of the metal. Fig. 1 shows the fracture of 446 SS tested at 450°C (840°F); whereas, Fig. 2 is the fracture for 446 SS tested at 600°C (1100°F). Figs. 3 and 4 show the cross-section at two magnifications of 446 SS tested at 450°C (840°F). Note the 45° shear plane etched out in the photograph of higher magnification. Figs. 5 and 6 show the cross-section at two magnifications of 446 SS tested at 600°C (1100°F). Note the elongated grains in the photograph at higher magnification.

The other new alloy, Inconel 671 (50 nickel-50 chromium), showed a large decrease in property values when tested at 600°C (1100°F) as compared to the property values obtained from a test at 450°C

(840°F). The two inconel specimens 671 tested at 600°C (1100°F) fractured
in a brittle manner with secondary cracks along the reduced sector much
the same as seen for 310 SS when tested at 540°C (1000°F) or 600°C
(1100°F). No published data for elevated temperature properties of
elongation and reduction in area could be found for Inconel 671, but
the room temperature elongation and reduction in area are 25% and
30%, respectively. Short time tensile strength of Inconel 671 was
reported as 690 MPa (100,000 psi) at 427°C (800°F) and 552 MPa
(80,000 psi) at 649°C (1200°F); whereas, our tests revealed tensile
strengths of 425 MPa (61,600 psi) and 416 MPa (60,300 psi) when
tested at 600°C (1100°F) at a slow strain rate of 10^{-6} s^{-1}.

Figs. 7 and 8 show the cross-section of the two Inconel 671 specimens
tested at 600°C (1100°F). Both figures indicate that the ductility
is low, that is, there is very little, if any, necking. In fact,
Fig. 7 shows that the specimen fractured in an area toward the
shoulder rather than at the minimum diameter. Figs. 9 and 10 are
etched cross-sections of Inconel 671 specimens. These
photomicrographs indicate that another phase was formed when Inconel
671 specimens were tested at 600°C (1100°F) at a strain rate of 1 X
10^{-6} s^{-1}. This phase, according to International Nickel Co., is
alpha chromium, a brittle phase. The cracks and fissures in the
specimens seem to occur only in the brittle alpha chromium phase,
thus accounting for the reduction in property values as seen in table
2 when compared to table 1. Fig. 11 is a photomicrograph of the
etched cross-section of the Inconel 671 specimen tested at 450°C
(840°F). This photomicrograph indicates that some necking did occur
and that the fracture occurred on the 45° shear plane. Fig. 12 shows
that there is very little, if any, alpha chromium formed in Inconel
671 when tested at 450°C (840°F) at a strain rate of 1 X 10^{-6} s^{-1},
thus accounting for the higher ductility as seen in table 1.

The above mentioned brittle failure of Inconel 671 and the previously
reported brittle failure of stainless steel type 310 indicate the
possibility of premature brittle failure of stressed components
manufactured of these alloys when used at elevated temperatures
— apparently, regardless of the environment to which they are exposed.

Plans: Continue testing alloys in oxidizing coal gasification atmosphere.

Figure 1. Scanning electron micrograph of a 446 stainless steel
specimen tested at 450°C (840°F) at a strain rate of $1 \times 10^{-6} s^{-1}$
in ultra-pure helium. 20X.

Figure 2. Scanning electron micrograph of a 446 stainless steel specimen tested at 600°C (1100°F) at a strain rate of $1 \times 10^{-6}s^{-1}$ in ultra-pure helium. 20X.

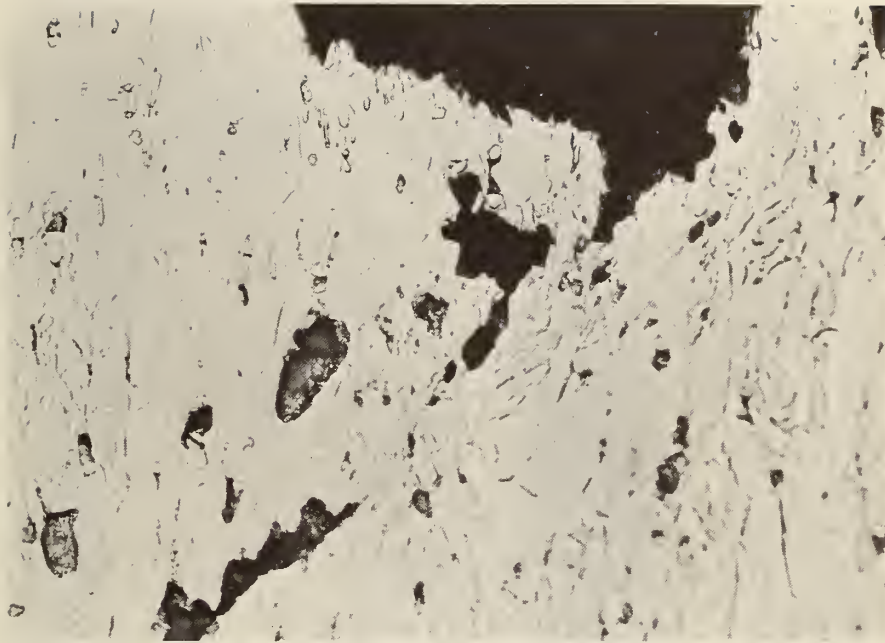Figure 3. Photomicrograph of the etched cross-section of the 446 stainless steel specimen in Figure 1. 25X.

Figure 4. Photomicrograph of the etched cross-section near the fracture of the 446 stainless steel specimen in Figure 1. 500X.
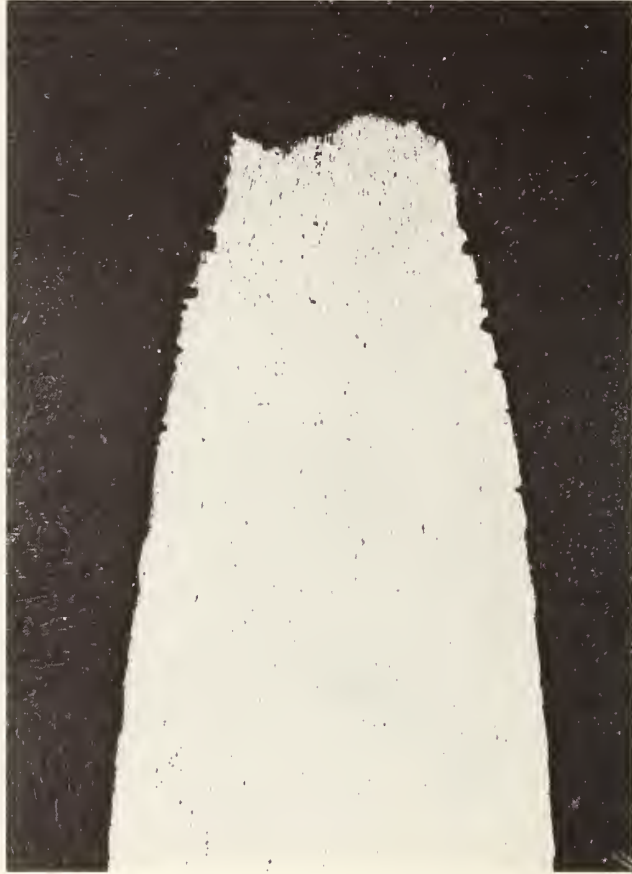
Figure 5. Photomicrograph of the etched cross-section of the 446
stainless steel specimen in Figure 2. 25X.

Figure 6. Photomicrograph of the etched cross-section near the
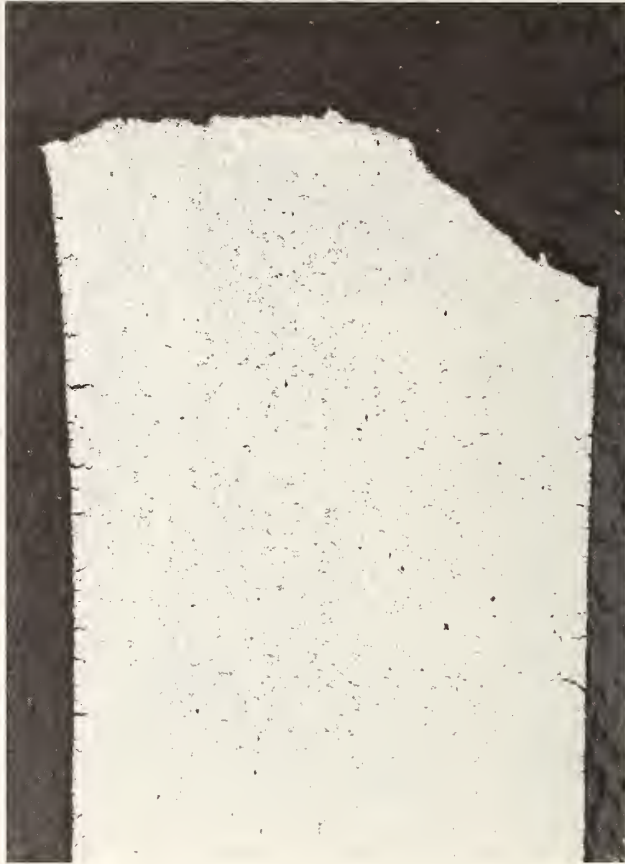fracture of the 446 stainless steel specimen in Figure 2. 500X.

Figure 7. Photomicrograph of the etched cross-section of the fractured Inconel 671 specimen tested at 600°C (1100°F) at $1 \times 10^{-6}s^{-1}$ in ultra-pure helium. 25X.
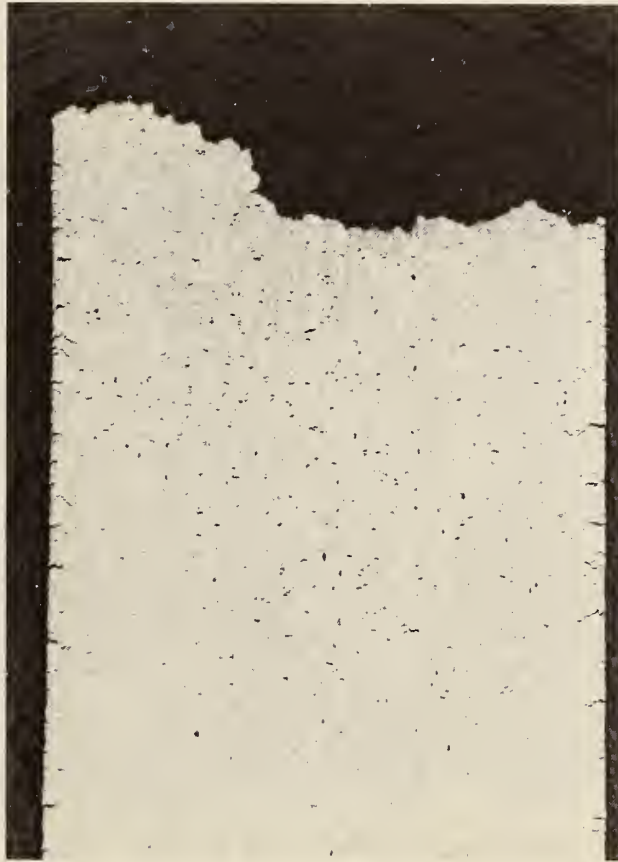
Figure 8. Photomicrograph of the etched cross-section of the fractured
           Inconel 671 specimen tested at 600°C (1100°F) at 1×10^{-6} s^{-1}
           in ultra-pure helium.   25 X

15

Figure 9. Photomicrograph of the etched cross-section of the
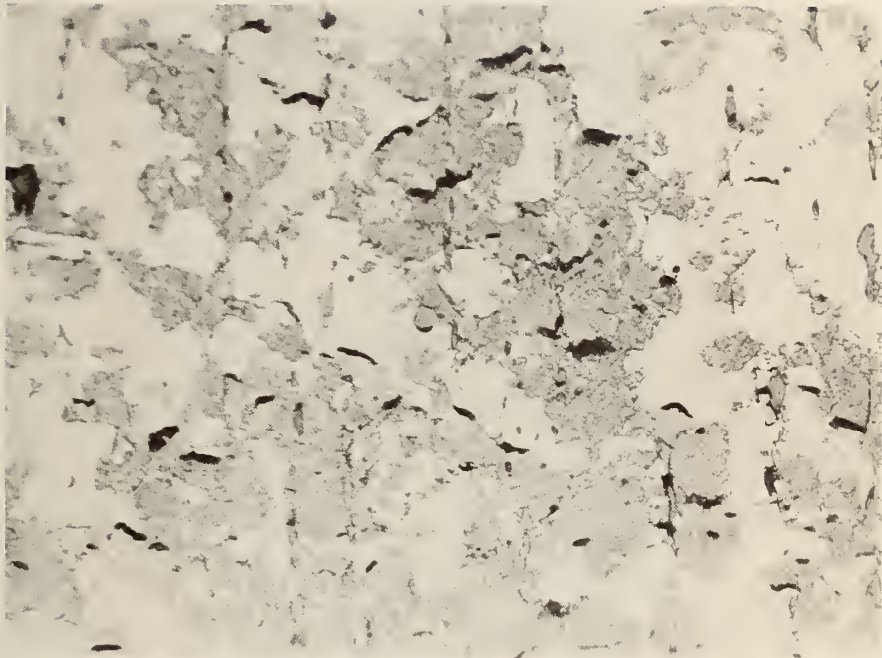Inconel 671 specimen in Figure 7. 500X.

Figure 10. Photomicrograph of the etched cross-section of the
Inconel 671 specimen in Figure 8. 500X.

Figure 11. Photomicrograph of the etched cross-section near the fracture of an Inconel 671 specimen tested at 450°C (840°F) at $1 \times 10^{-6}s^{-1}$ in ultra-pure helium. 25X.

Figure 12. Photomicrograph of the etched cross-section of the
Inconel 671 specimen in Figure 11. 500X.

b.   Pre-Cracked Fracture Tests (J. H. Smith, 312.01)

Progress: Further work was done to optimize the design of the wedge-loaded
cantilever-beam test specimen for use at elevated temperatures. For test
materials of interest, the decrease in the elastic-modulus at elevated
temperatures causes a substantial decrease in the elastic stress-intensity
factor. This decrease in modulus cannot be fully compensated for by
increases in thermal expansion or decrease in yield strength of the test
specimen so that the stress-intensity will remain relatively constant as
temperatures increase. Of equal significance is the fact that the stress-
intensity in a wedge-loaded double cantilver beam specimen will increase
as the specimen is cooled from elevated temperatures back to room temperature
after testing. Several other test specimen configurations have been
investigated to determine if the stress-intensity can be made less sensitive
to changes in temperatures of the specimen.

Additional elastic stress analysis was done to evaluate various modifications
to the wedge loaded DCB specimen. For selected materials of interest in coal
conversion systems, such as 310 stainless steel, the decrease in stress
intensity due to increase in temperature can be limited to approximately
10 percent up to a temperature of 1000°F and to about 20 percent up to 1200°F.

Plans: The wedge-loaded cantilever beam specimen will be optimized so that
the stress-intensity is accurately defined for several materials of interest
at a series of selected temperatures. Several additional specimens will be
analysed to determine if they are more suitable for use at elevated
temperatures.

The elastic-plastic stress analysis of the wedge-loaded double cantilever
beam specimen to determine the stress-intensity and J-integral values will
be initiated. This will be done using stress-strain curves for specific
test materials of interest at selected temperatures.

Continued analysis of the DCB and modified DCB specimen configurations will
be carried out to optimize the specimen design and to develop a specimen
that exhibits a constant stress-intensity, K, over a reasonably wide range
of temperatures for materials of interest. Several specimen configurations,
other than the DCB specimen, are being evaluated to extend the useful
temperature range of the specimen. Elastic-plastic stress analyses of the
specimens will be initiated to extend the use of the specimen beyond the
range of applicability of the elastic analyses.

2. Ceramic Deformation, Fracture and Erosion (E.R. Fuller, Jr.,
S.M. Wiederhorn, J.M.
Bukowski, D.E. Roberts,
and C.R. Robbins, 313.05)

Progress: The major effort of this past quarter has been directed to
the continued construction of a high-temperature, high-pressure mechanical
loader. Construction of a three-zone furnace assembly around the inner
environmental chamber has been completed along with the wiring of the
temperature controllers necessary for operation. A total of twelve
thermocouples have been placed in the unit so that the temperature
profile can be determined under actual operating conditions. Five of
these thermocouples are located in the inner environmental chamber. The
remaining thermocouples monitor the temperature profile throughout the
outer containment pressure vessel. Stainless steel baffles are used to
restrict convection currents and to lower the radiant heat transfer in
the inner chamber.

Several runs at atmospheric pressure have been made in a nitrogen
environment (low partial pressure of oxygen) to a temperature of 1000°C.
The temperature gradient inside the sample chamber could be controlled
to 5°C or less. Heat losses to the outer vessel under these conditions
were found to be minimial even at the maximum operating temperature of
1000°C. A failure of a temperature controlling thermocouple resulted in
the disassembly of the outer pressure vessel for replacement. The exact
cause of failure has not been diagnosed, but because of the low partial
pressure of O_2 in the environment, "green-rot" of the chromel-alumel
(type K) thermocouples is suggested. Presently, sheathed thermocouples
are being prepared for use in the unit, and will be installed once the
checkout phase is completed.

As part of the mechanical testing after hydrothermal exposure, two
lengthy exposure tests were conducted this quarter. In one, high
alumina refractory concrete specimens were heated to a temperature
of 910°C (1670°F), after which the steam pressure was increased to 7 MPa
($\sim$ 1000 psi). The time of exposure at temperature was 330.5 hours.
These high alumina specimens showed an increase in flexural strength
from 19.0 $\pm$ 1.2 MPa (2,750 $\pm$ 180 psi) to 29.2 $\pm$ 6.7 MPa (4,240 $\pm$ 970
psi). In the other exposure test, high alumina specimens were heated to
410°C following the saturated vapor curve to a pressure of 7.0 MPa.
After a 46 hour exposure at 410°C, the temperature was increased (at
constant pressure) to 610°C for a 43 hour exposure. Following this
exposure, the temperature was increased to 910°C for a 335 hour exposure.
These specimens showed a similar strength increase to 31.0 $\pm$ 7.5 MPa
(4,490 $\pm$ 1,090 psi). Mineral phases were predominantly α-alumina, and
$CaO.2Al_2O_3$, but some hydrated phases apparently formed during cooling
from temperature. It is the formation of these hydrated phases that are
most likely responsible for the increase in strength shown by the concrete
specimens after hydrothermal exposure.

21

Exposure studies on high alumina concrete in a 70% H_2O-30% CO_2 environment have also been initiated this quarter. In this set of experiments, the pressure vessels are charged with calculated amounts of both CO_2 and H_2O at room temperature so that the pressure at the exposure temperature is approximately 7 MPa ($\sim$1000 psi). Cursory data on high alumina concrete exposed at 610°C for 42 hours showed only a slight increase in room-temperature flexural strength from 15.6 $\pm$ 0.7 MPa (2,2262 $\pm$ 102 psi) to 20.5 $\pm$ 1.5 MPa (2,973 $\pm$ 218 psi). X-ray analysis also showed the formation of calcium carbonate in the refractory concrete specimens.

Plans: Construction of the high pressure vessel for mechanical testing in simulated gasification environments will be continued. Once the heat zone has been fully characterized as a function of temperature and pressure, the pressure balancing unit will be installed. On satisfactory operation of both the heating and pressure system, the load system will be installed and the operation of the hydraulic ram, bellows and load cell will be checked using refractory concrete specimens at ambient, high, and low temperatures, and at pressure. Finally the water injector will be installed and the system will be operated with steam in the environmental chamber. When this check-out scheme is completed, the system will be operational and systematic studies on refractory concretes will commence.

Exposure studies will continue on both the high-purity alumina and the calcined flint clay castable refractories for gas mixtures of 70% H_2O - 30% CO_2 and 30% H_2O - 70% CO_2. Following the completion of these studies, a gas mixture of approximately 15% CO_2, 20% CO, 25% H_2, and 40% H_2O by volume will be used. With the exception of H_2S and NH_3, the latter mixture will fully simulate the coal gasification environment. As in the previous studies, a range of temperature, pressure and exposure time will be investigated. The erosion resistance at room temperature of exposed refractory concrete specimens will also be characterized. X-ray diffraction and scanning electron microscopy will be used to identify important phase changes that occur during exposure.

3. Chemical Degradation of Ceramics

a. Reactions and Transformations (F. A. Mauer and C. R. Robbins, 313.06)

Progress: During the past quarter assembly of the pressure vessel for x-ray diffraction measurements was completed. External heaters were installed and a safety shield was constructed to limit damage in case of failure of the pressure vessel.

The B_4C x-ray windows were judged to be too rough for satisfactory sealing with metal gaskets even after they had been ground to the desired dimensions. They were sent to the optical shop for polishing, and, since the surface still appeared somewhat grainy, they were plated with gold to provide an improved seat for the gaskets. The gasket seats in the stainless steel pressure vessel were lapped with diamond paste to remove tool marks before final assembly of the x-ray ports containing the B_4C windows.

The initial pressure test was carried out with N_2 gas to a maximum pressure of 1400 psig. The pressure dropped to 700 psig during the following 20 hours, indicating that some leakage occurred possibly as a result of porosity of the hot-pressed B_4C windows. This amount of leakage can easily be tolerated.

Calibration runs with a saturated steam atmosphere have been carried out to determine the power input required to maintain various temperatures. These have proved to be quite time consuming because of the time required to establish equilibrium. The three external heaters provide a maximum of 650 watts distributed over the top, bottom, and sides of the pressure vessel. Approximately one inch of fiber insulation surrounds the heaters. A power input of 220 watts is sufficient to maintain a wall temperature of 300°C when the internal heater is off, but because of the mass of the pressure vessel (8.6 kg), the additional power is needed to reach operating temperature within one hour. When power is applied to the internal heater the input to the external heater must be reduced by a like amount to avoid an increase in wall temperature. For inputs in excess of 200 watts, it is no longer possible to limit the wall temperature to 300°C with the present arrangement. When the wall temperature was allowed to reach 379°C, a loss of pressure occurred, presumably because of failure of the Teflon thread sealant ($T_{max} \sim 250$°C) at the base of the water reservoir. This seal can be relocated to a region of lower temperature or eliminated altogether.

With the present internal heater which is wound with 0.032 in. diameter 80% Pt - 20% Rh wire we are limited to 450 watts input, which is sufficient to reach a sample temperature of 900°C. To reach the specified temperature of 1000°C while maintaining a wall temperature of 300°C it will be necessary to provide additional insulation around the furnace core to reduce heat transfer by convection. We plan to cast the furnace core in a block of alumina with a bubbled-alumina aggregate, which can be done with no change in the design of the pressure vessel itself.

23

Additional standard patterns of relevant cement phases have been recorded by the energy dispersive powder diffraction method. The patterns are shown in Figures 1-5. The conditions are the same as for the eight patterns included in our previous quarterly report (January-March 1977). The identification of peaks is not shown in Figure 5 (CAS_2) because of the complexity of the pattern, although the indexing has been carried out.

Plans: Modifications to the internal heater to reduce heat transfer to the outer wall of the pressure vessel will require approximately one month to complete. Only a moderate reduction is required and x-ray diffraction measurements are expected to begin during August 1977.
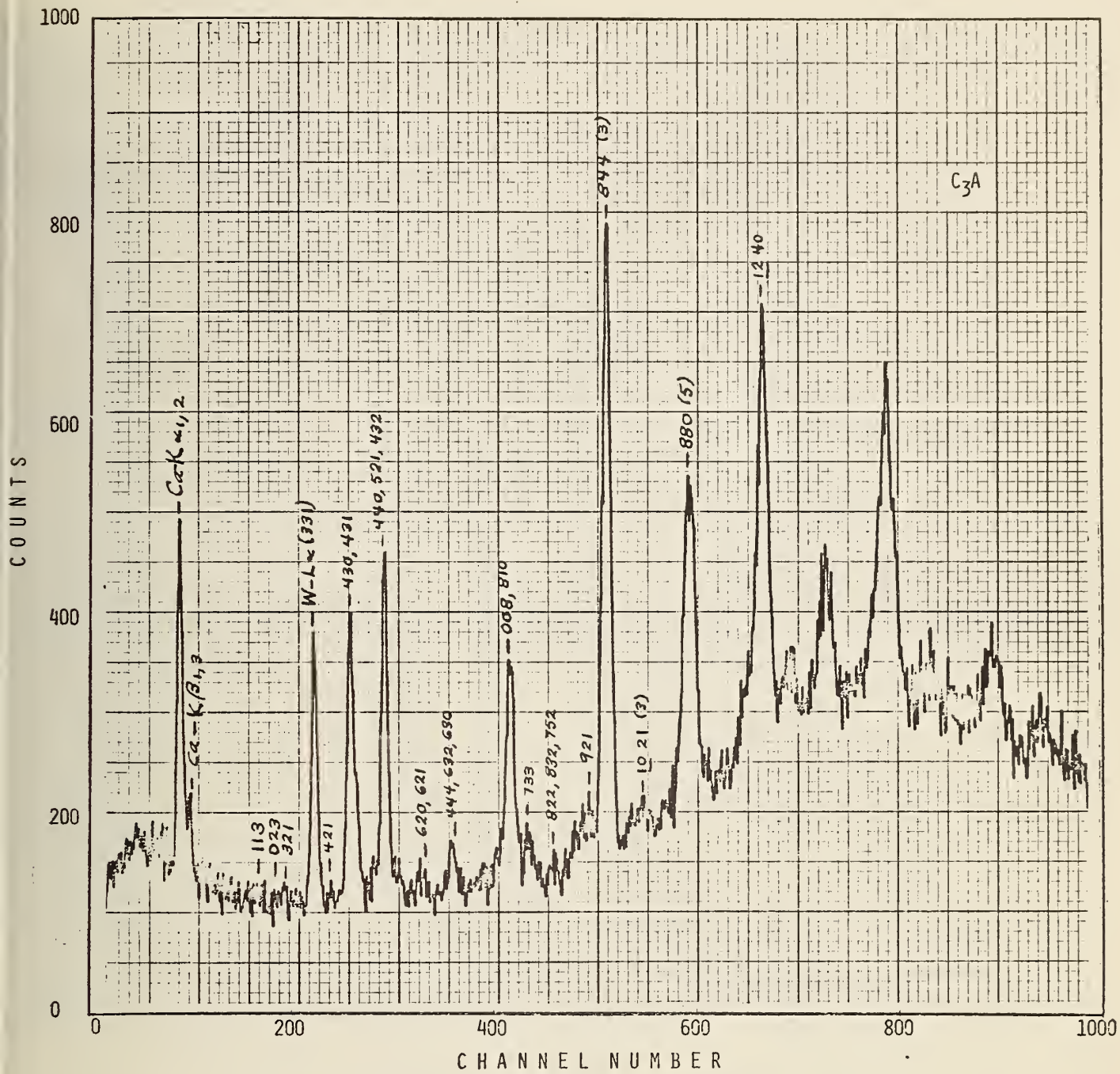
Figure 1.   EDXD pattern of C₃A.
(C = CaO, A = Al₂O₃)

25
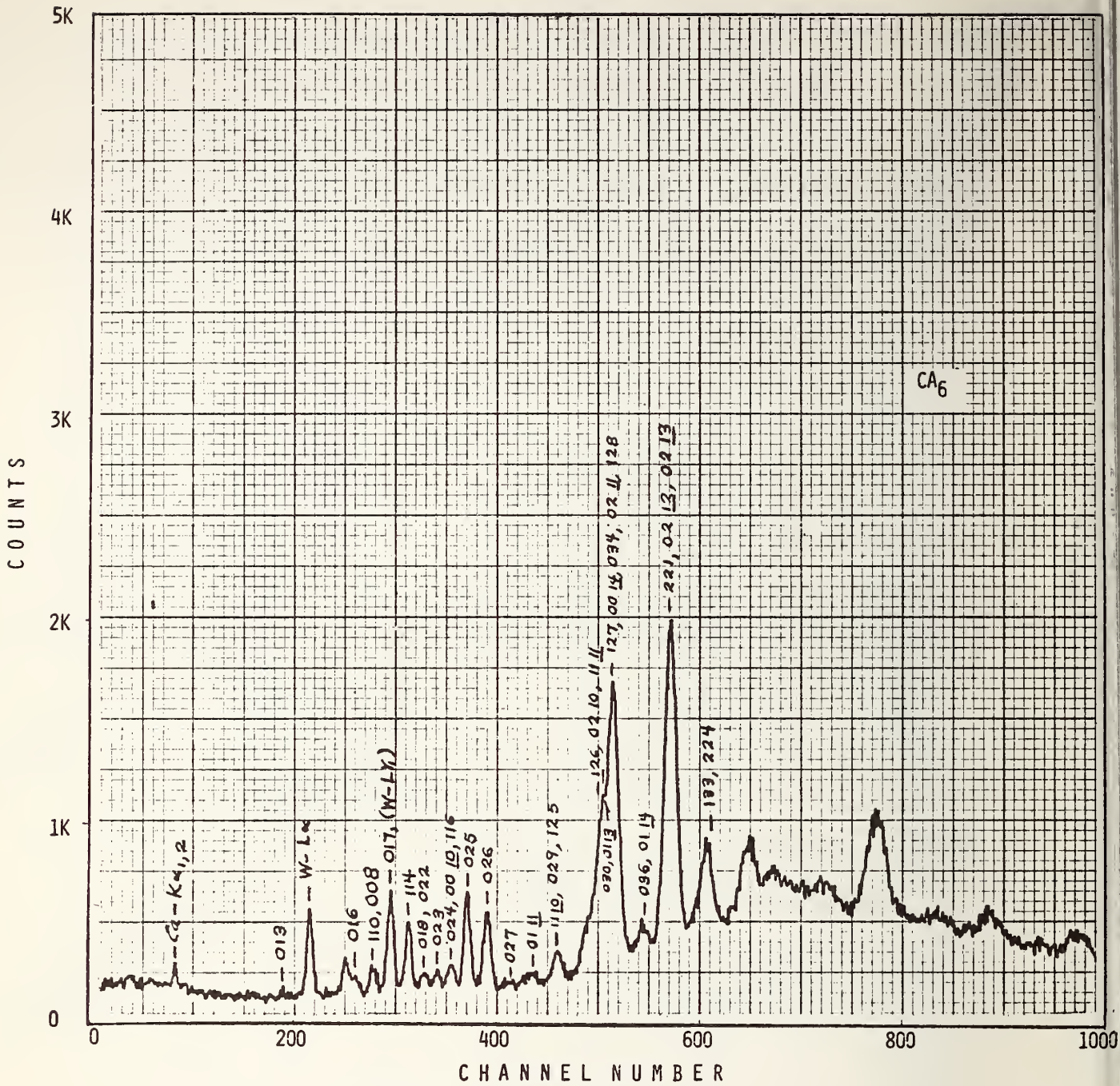
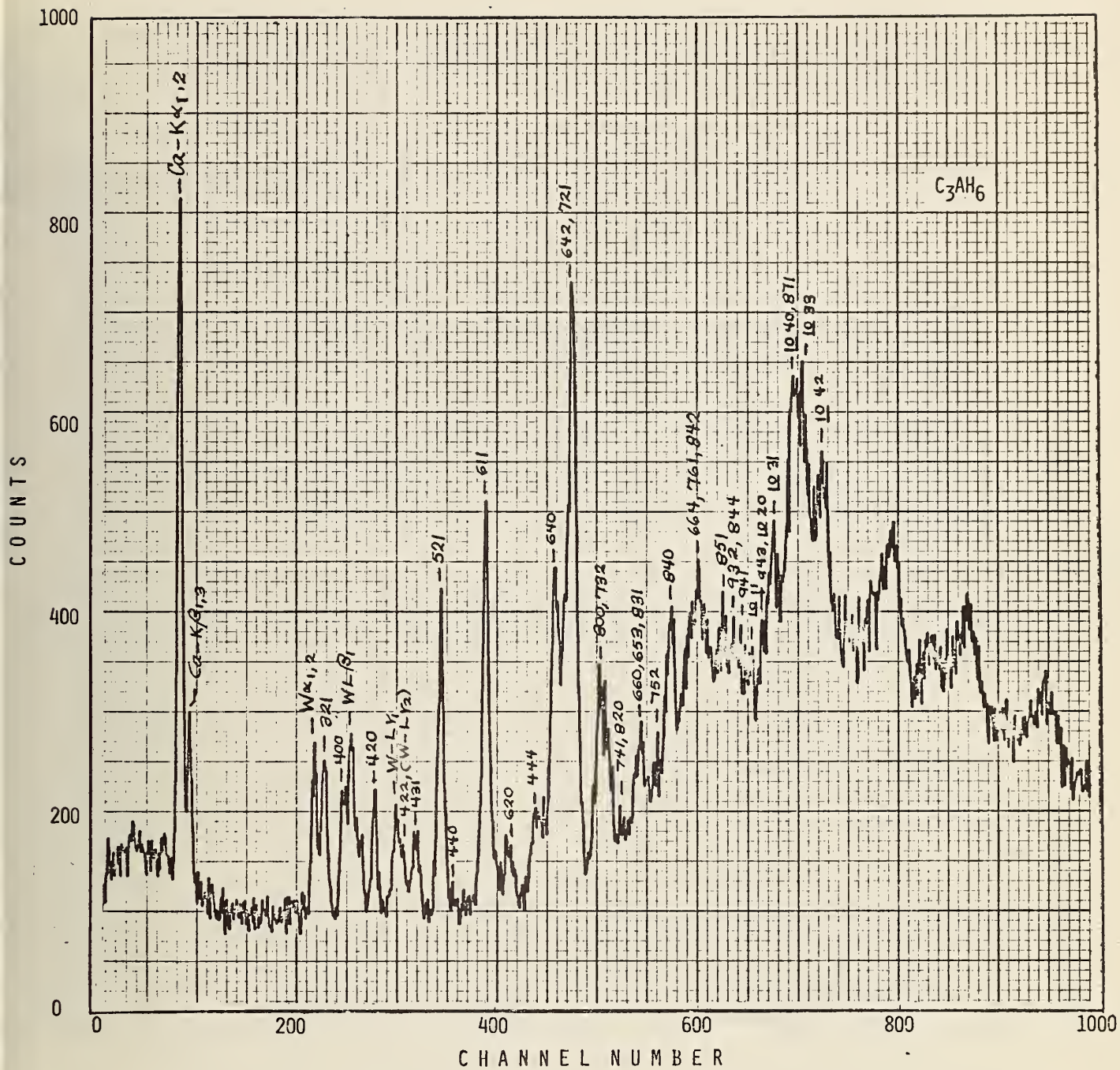Figure 2.   EDXD pattern of CA_6.

($C = CaO$, $A = Al_2O_3$)

26

Figure 3.   EDXD pattern of C_3AH_6.
          (C = CaO, A = Al_2O_3,
          H = H_2O)
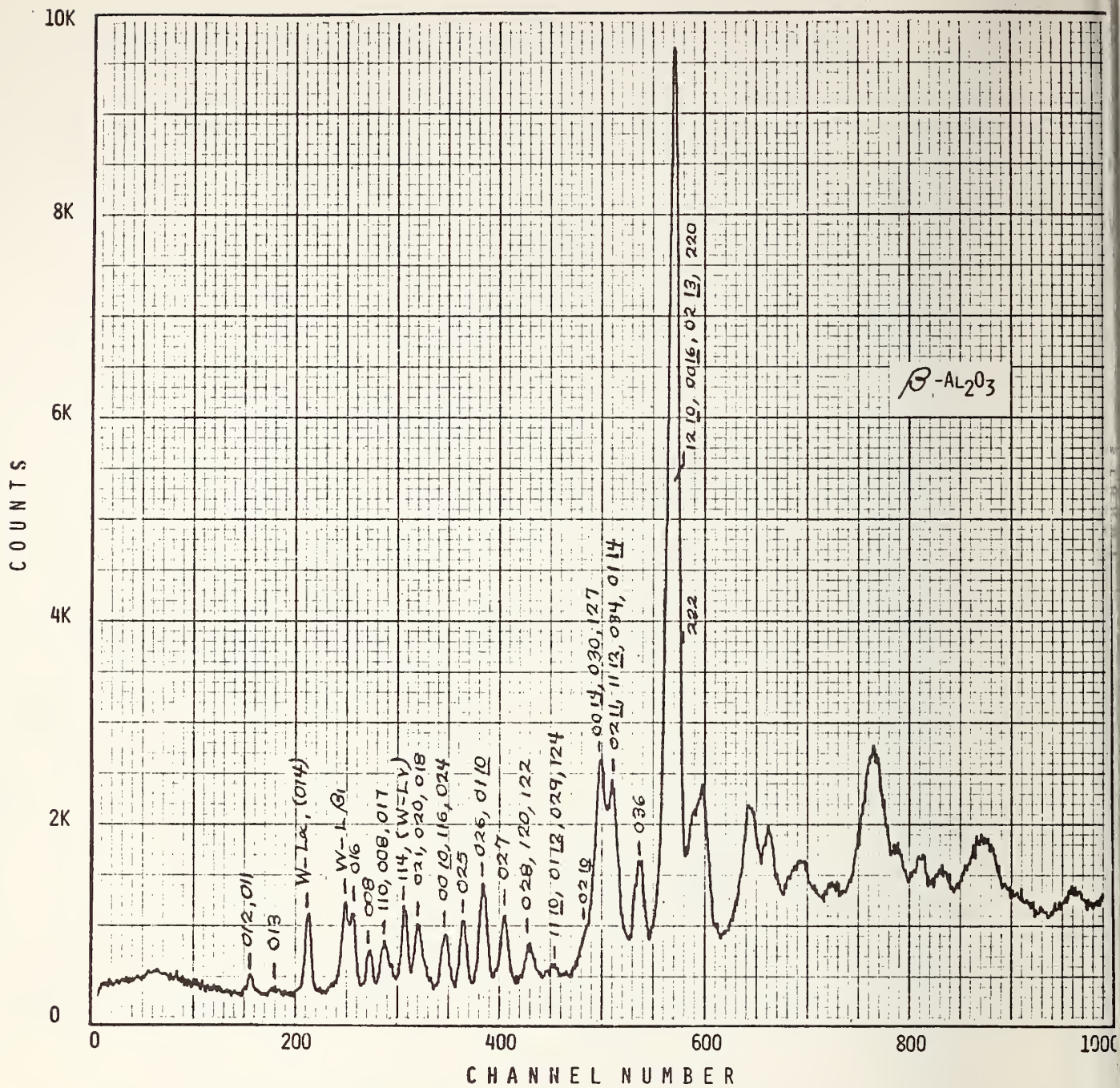
27

Figure 4.   EDXD pattern of β-Al$_2$O$_3$.
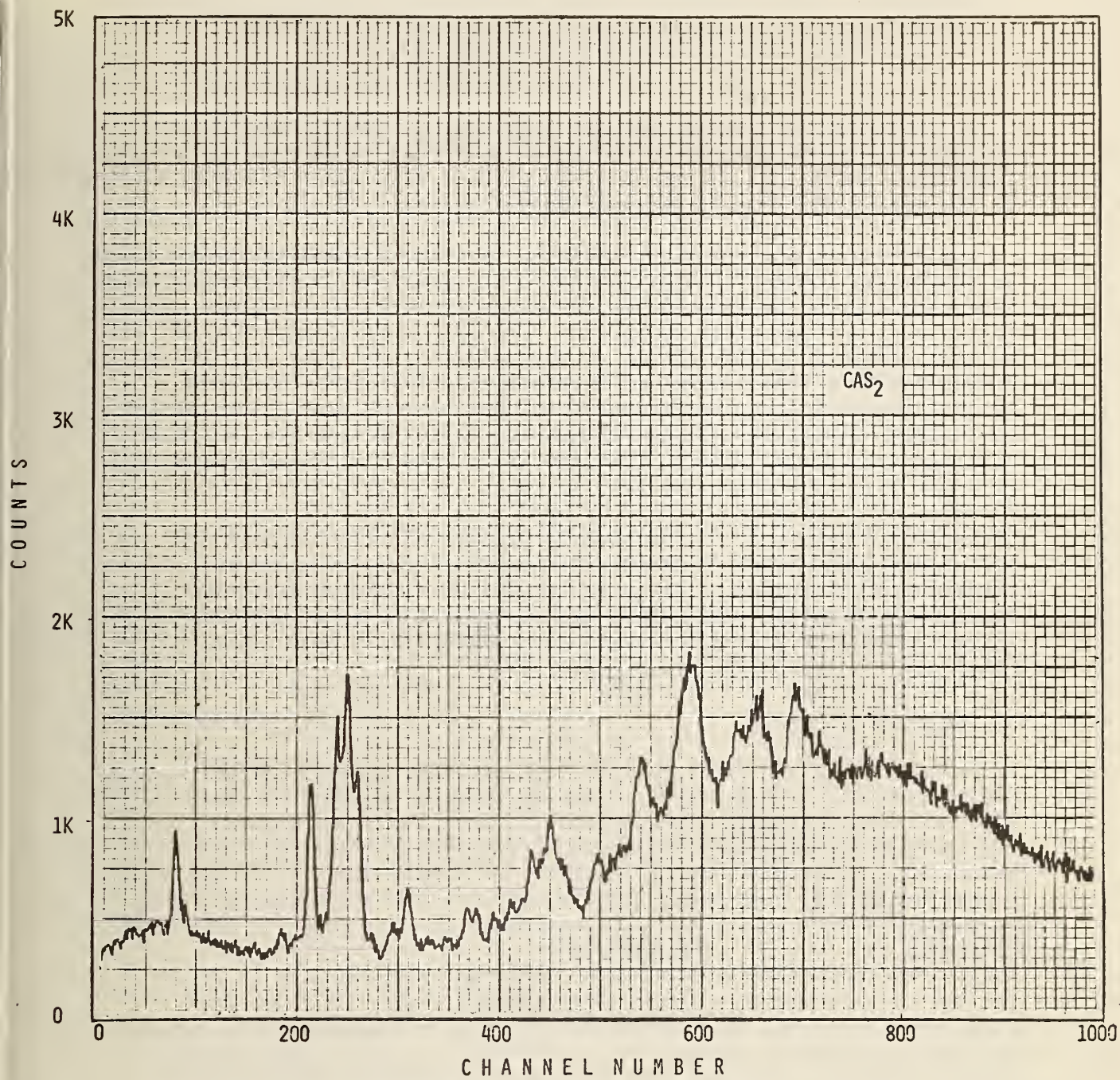
28

Figure 5.   EDXD pattern of CAS_2.

b. Slag Characterization (W.S. Brower, J.L. Waring, 313.03 and
                          D.H. Blackburn, 313.02)

<u>Progress</u>:

1. <u>Design of High Pressure/Temperature Vessel</u>

    A high pressure vessel potentially capable of achieving temperature
of 1350°C and 100 psi of steam has been designed and constructed at NBS.
This apparatus is to be employed in the measurement of viscosity of
molten slag at high steam pressures. The apparatus (Figures 1, 2)
was fabricated from 304L ss and is approximately 24" long and 10" in
diameter with a total volume of approximately 2072 in^3. The main
body of the vessel was fabricated from Schedule 40S pipe. The top
and bottom (Figure 3) 10 inch flanges are class 300 and are fastened
with sixteen one inch bolts. The two side ports with cover plates
are also class 300 which are held in place with eight 3/4" bolts.
The side ports (Figure 4) serve to introduce two massive copper
electrodes (Figures 5, 6) necessary to carry sufficient current to
heat a platinum heater in steam, while maintaining the pressure
integrity of the vessel. These electrodes are isolated from the
vessel body by mica. The copper electrode seal is made with the
flange using an "0" ring in conjunction with a split lock collar
(Figure 7) and retaining ring (Figure 8).

2. <u>Steam Generation</u>

    The steam used in the apparatus is generated internally by
vaporizing water using nine bayonet type heaters (Figure 9) which
together dissipate approximately 3600 watts. These heaters are
isolated from the internal pressure by three finned copper heat
exchangers (Figures 10, 11, 12). There are three heaters in each
copper radiator. The internal and external surfaces of the radiators
are pressure isolated by an "0" ring seal. At this point it should be
mentioned that all "0" ring seals employed in this apparatus are
fabricated from ethylene propylene. This material appears to offer
the best resistance to high pressure steam. Figure 11 shows the
relationship between the heaters and the heat exchangers. The bayonet
heaters are supplied power from a 10 KVA S.C.R. power supply used in
conjunction with a current adjusting type controller. These bayonet
heaters must be controlled since they in effect control the steam
pressure in the vessel. A baffle assembly (Figures 13, 14) is used
above the copper heat exchangers to reduce bumping caused by the
evolution of steam. A copper-copper constantan thermocouple is used
with this devise to monitor steam temperature, hence pressure. To
reduce radiative and convective cooling of the platinum heater, a

refractory castable is placed around the heating element. To minimize refluxing H_2O, three shields are placed above the specimen.

3. Temperature Measurement and Control

The high temperature to which the samples are to be heated is achieved by passing high current through a platinum cylinder fabricated from platinum sheet 1 mm thick. The cylinder is six inches in length and 2 1/2 inches in diameter. This cylinder has two tabs or ears welded on the long axis 180° apart. The total radiating surface of the heater is approximately 29 in. These tabs are compressed between two copper plates which comprise the ends of the copper electrodes. These copper plates have been gold-plated to minimize contact resistance in the presence of steam.

The platinum cylinder is heated with a controlled 10 KVA power supply used in conjunction with a 100-1 step-down transformer. The temperature of the heating element is measured with a Pt-Pt-10%RH thermocouple. This system is estimated to control the temperature of the melt to ±10°C.

4. High Temperature/Pressure Viscometer

The crucible containing the molten slag is made of 0.025 inch thick platinum and is 1 1/2 in diameter and 3 in. high. The crucible is mounted and centered on an alumina pedestal which extends into a shaft coupler attached to the drive mechanism (Figure 15). The viscosity bob is 12.5 mm in diameter, 50 mm in length with 45° tapered ends and is suspended by a platinum rod.

The spindle is suspended in the vessel with a phosphor-bronze wire which serves as a torsion member. At the lower end of the torsion member a permanent magnet is attached and moves as the torsion member is twisted. This magnet movement is detected by a ferrous metal detector located outside of the vessel. The driving mechanism (Figure 15) which turns the shaft and crucible consists of a 1/4 H.P. electric motor which drives a right angle gear reduction mechanism. The reduction ratio is 48-1. The shaft speed is variable from 2 to 44 rpm. The shaft enters the pressure vessel through a ethylene propylene "O" ring seal. The rate of rotation of the shaft assembly is monitored with an electronic tachometer.

5. Experimental Methods

The appratus described previously is calibrated at room temperature with a standard of known viscosity by measuring the angular deflection of the bob and noting the speed at which the crucible was rotating. A

viscosity standard must be selected which approximates the viscosity of the molten test slag. The liquids used for calibration were Dow Corning silicone fluids which have viscosities of 58,560 centipoises and 12,500 centipoises, respectively. The deflection θ of an inner bob in a rotating fluid is directly porportional to the viscosity η of the fluid and the angular velocity ω of the outer rotating crucible

$$\theta = C\omega\eta$$

where C = constant of porportionality depending on the geometry of the apparatus. The angular deflection θ of an unknown liquid can be compared with that of a standard of known viscosity by:

$$\frac{\theta_1}{\theta_2} = \frac{\eta_2 \omega_2}{\eta_1 \omega_1} \quad \text{or} \quad \eta_2 = \eta_1 \frac{\theta_2 \omega_1}{\theta_1 \omega_2}$$

where η_2 is the unknown viscosity.

Having the apparatus calibrated, the specimen is placed in the vessel. In a conventional viscosity apparatus, uncomplicated by the presence of a pressure vessel the specimen is melted and elevated to a sufficient height to immerse the bob. However, in this apparatus because of the restrictions imposed by pressure the slag will be melted (bob in place) in another furnace in air and this unit will be placed in the proper position in the pressure vessel. At this point the steam will be generated. Then the power will be turned on to remelt the slag. Several measurements will be taken with the shaft rotating in the clockwise direction and several in the counter clockwise direction.

In the last quarterly report the viscosity of a naturally occurring slag derived from Montana Rosebud Ash was compared with several selected synthetic compositions. In the synthetic compositions the silica was allowed to vary from 30 to 50 weight percent. In the presence of steam it is felt that the most significant changes in viscosity will be due

to changes in the $\underset{\displaystyle O}{\overset{\displaystyle O}{O-\underset{|}{\overset{|}{Si}}-O}}$ bonding in the melt due to incorporation of

$(OH)^-$ ions. As SiO_2 is the component which most affects viscosity at ambient atmosphere this variation should show the greatest affect under steam pressures. When the composition of the atmosphere is varied, changing the partial pressure of oxygen, variations of iron oxide content might well prove to have a significant effect on the viscosity.

32

At atmospheric pressure typical coal slag viscosities have been found to remain essentially constant as the oxygen activity is decreased. However, increasing the oxygen activity over that of air tends to increase the viscosity with increased Fe^{+3} content of the melt.[*] Reducing atmospheres that are typical in coal gasifier environments are not expected to have a really significant effect on viscosity, however large variations in iron content of the slag may well influence the viscosity as the total amount of Fe^{+2} will be increased and might be expected to decrease the viscosity much the same as increased Ca^{+2} content.

[*] W. Capps, private communication.

Plans: Construction and assembly of the major components of the pressure vessel, viscosity apparatus, have been completed. Preliminary heating and steam generation will begin by the end of July. Operation will begin with one atmosphere steam pressure moving to progressively higher pressures.
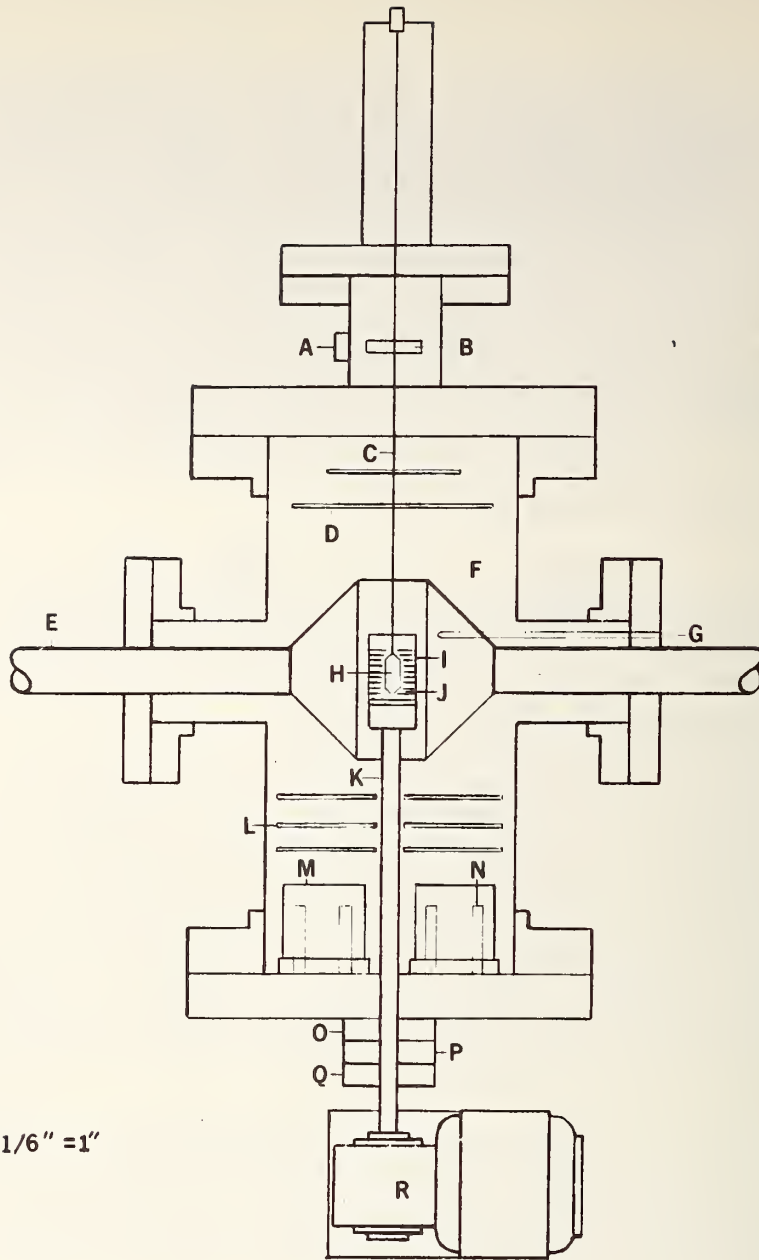
SCALE: 1/6″ = 1″

Figure 1. Full assembly schematic drawing of high pressure-temperature
viscometer.

A – position detector
B – magnet
C – torsion wire
D – water condensation shields
E – electrodes
F – heating elements
G – temperature control thermo-
couple
H – bob
I – crucible

J – molten slag
K – spindle
L – anti-convection baffle
M – heat exchangers
N – bayonet heaters
O – shaft seal
P – shaft cooling jacket
Q – shaft bearing
R – shaft drive mechanism

34
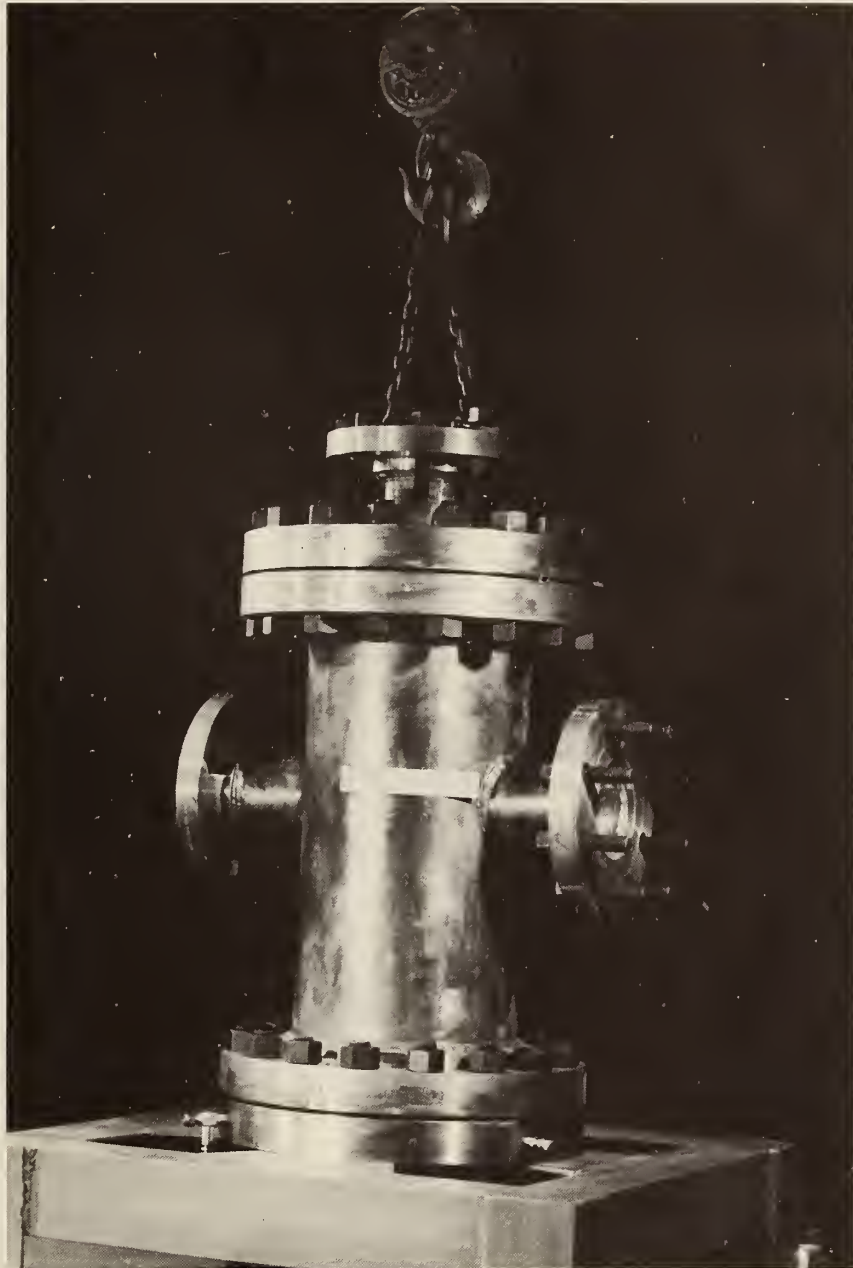
Figure 2.   Three quarter view of high pressure-temperature viscometer.
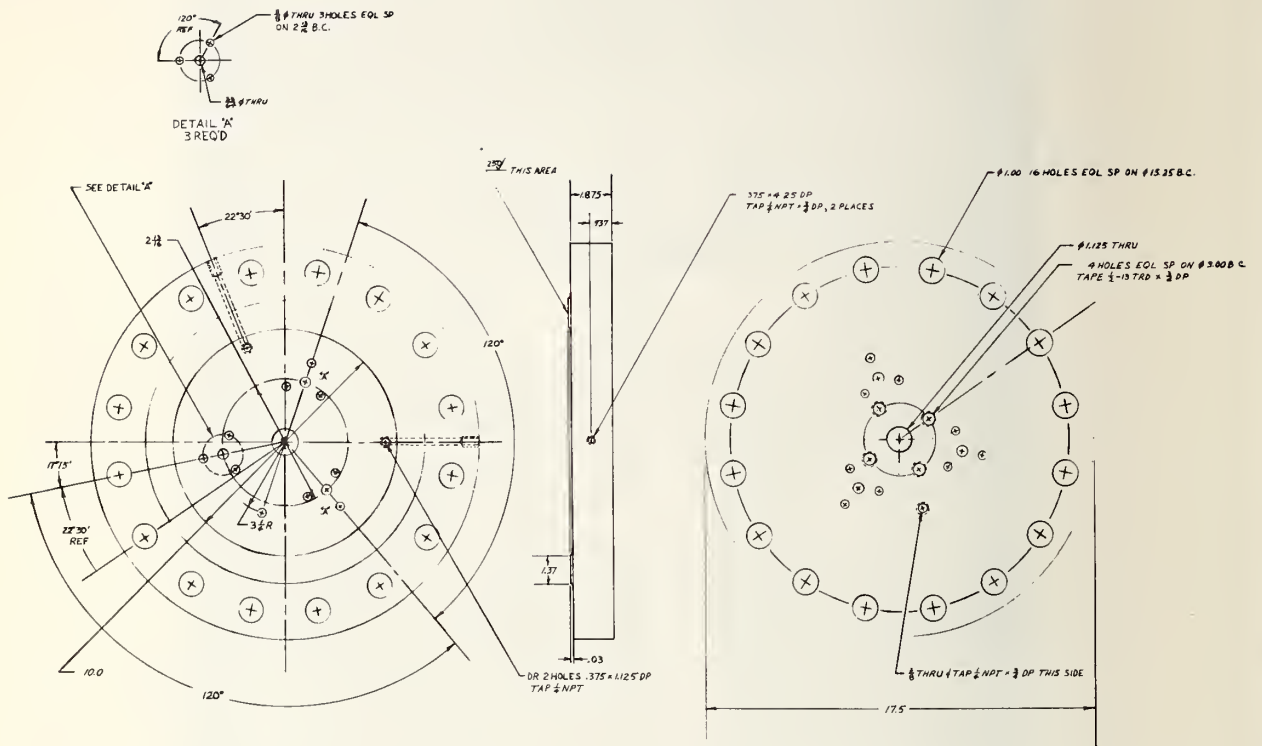
Figure 3. Drawing of lay-out of large bottom flange.
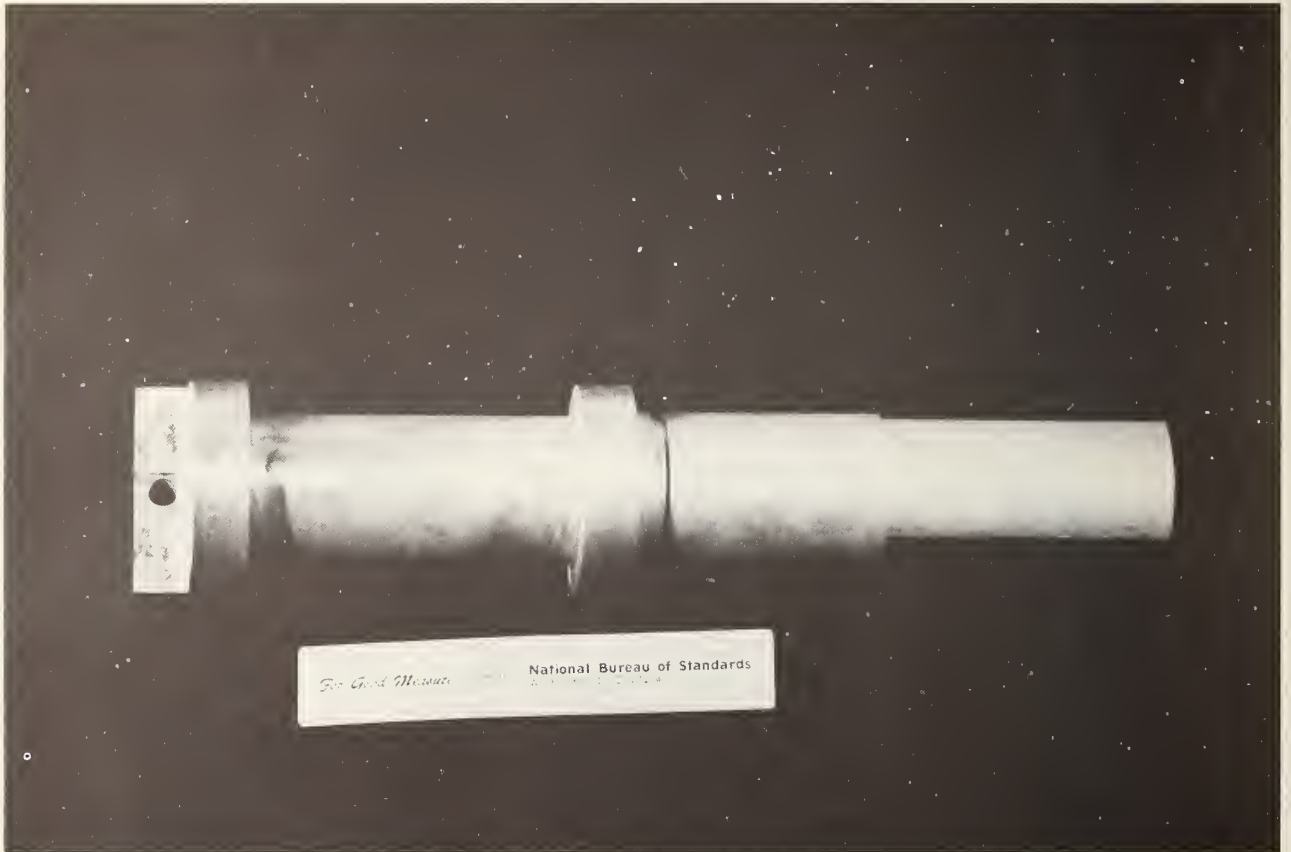
36
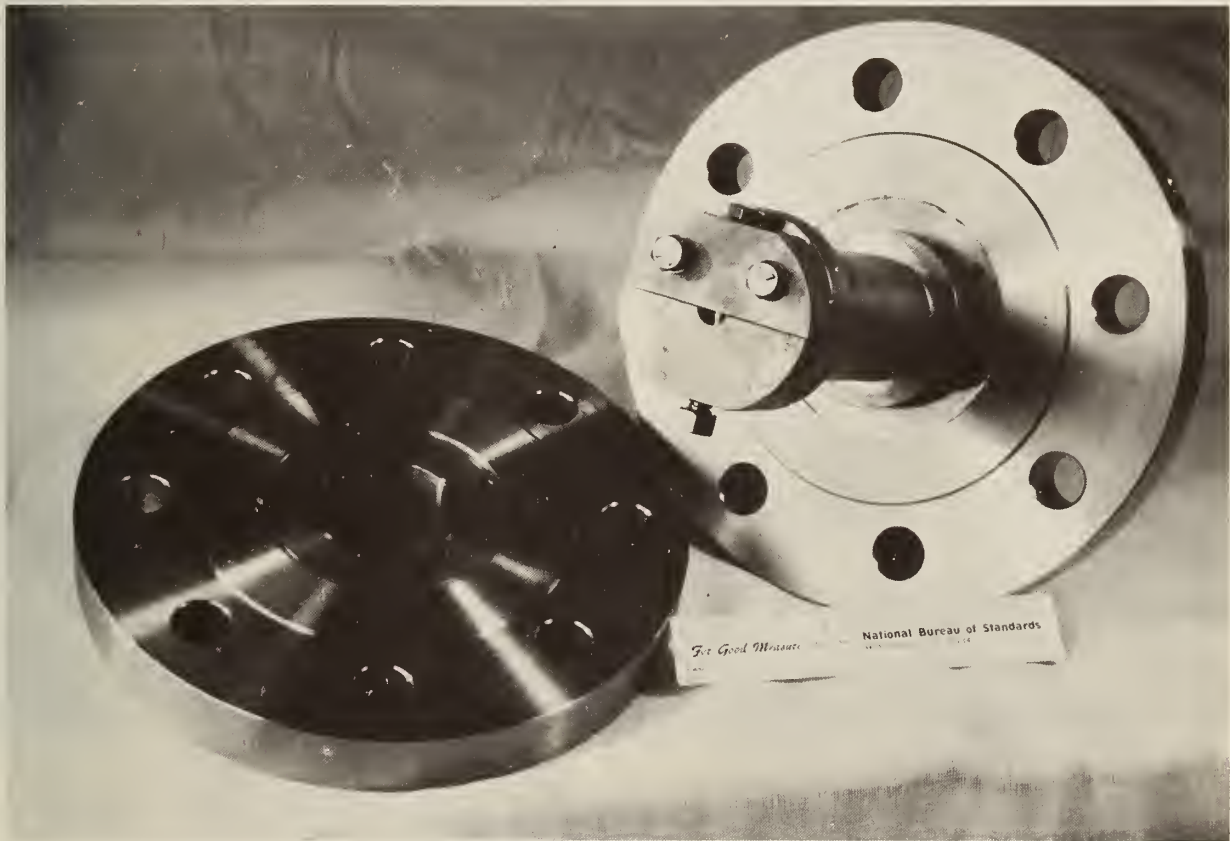
Figure 4.   Photo of electrode flange.
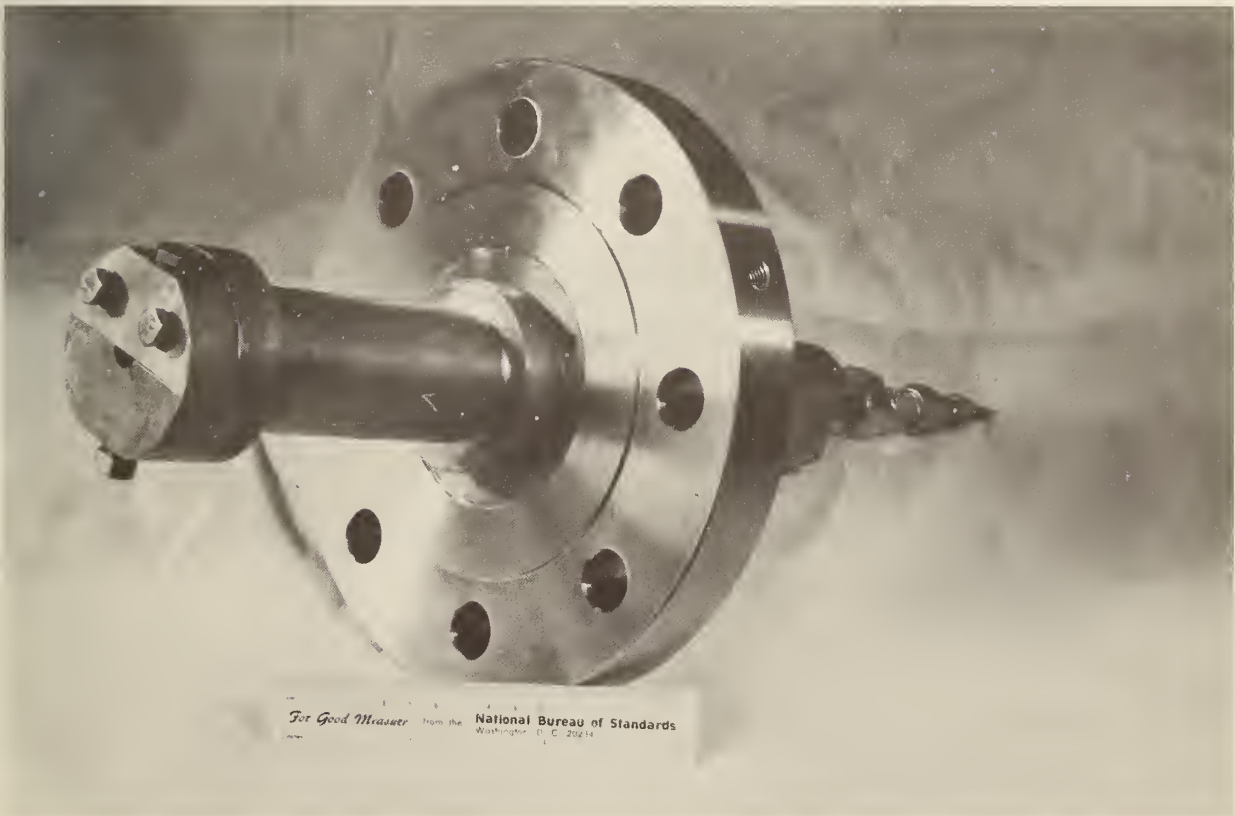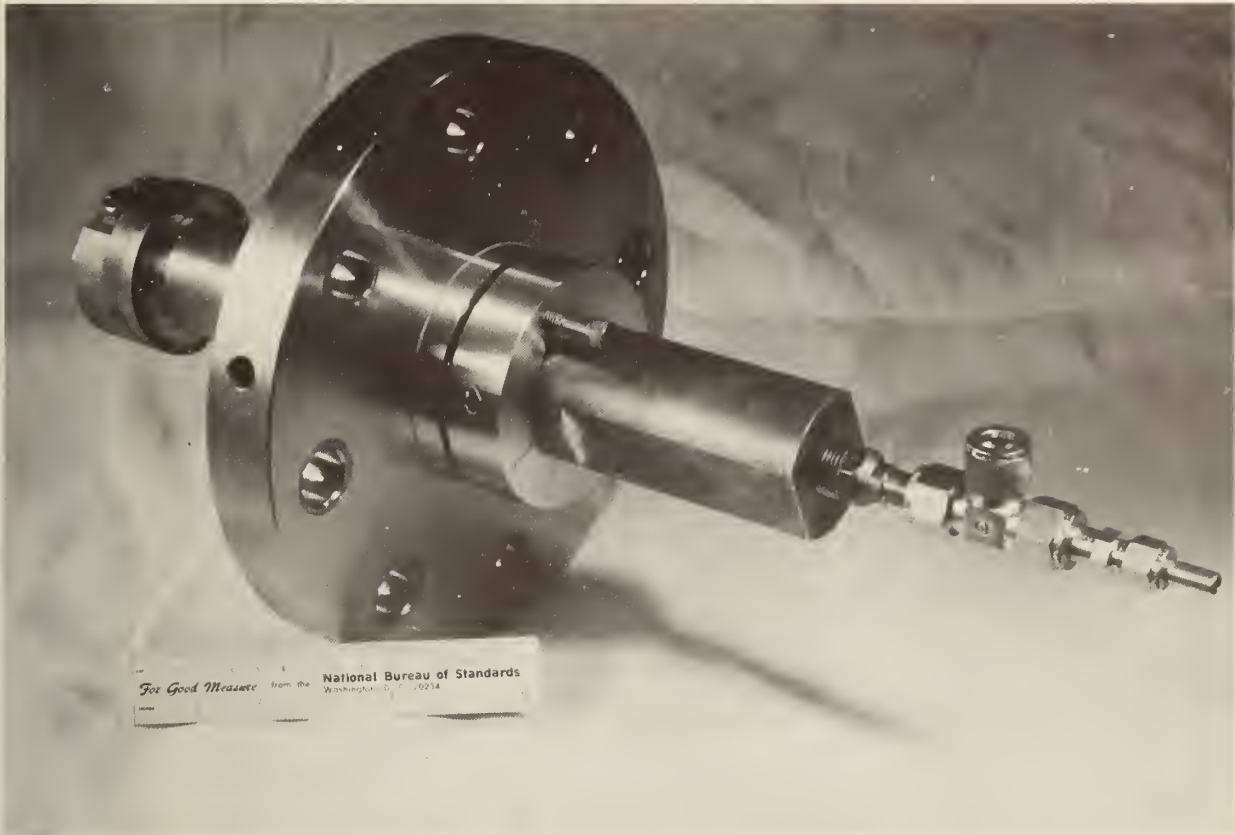
Figure 5a. Copper electrode.

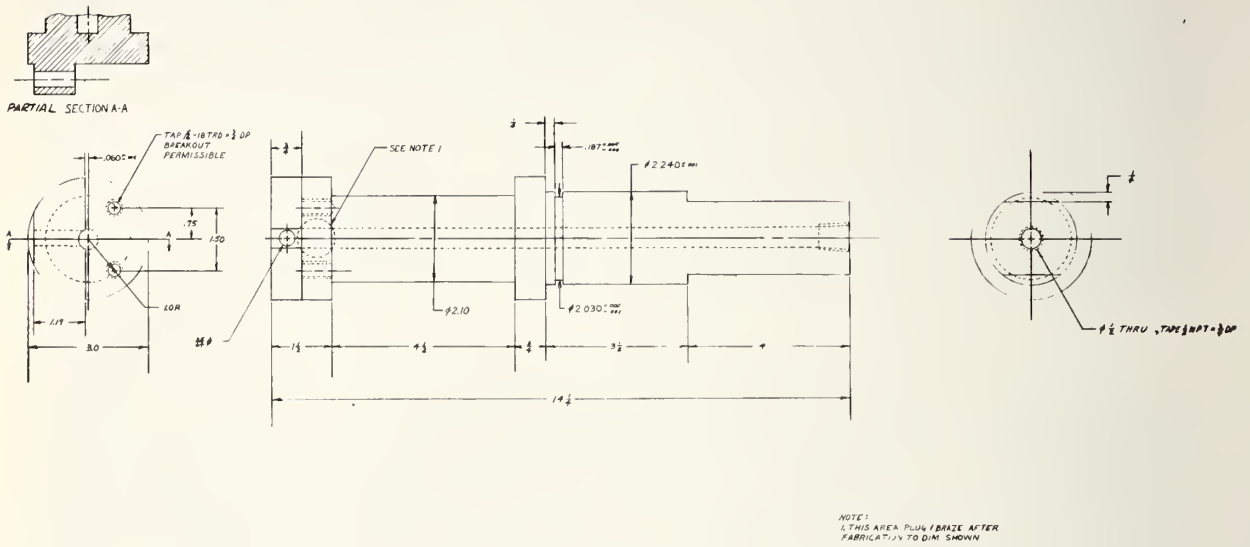Figure 5b. Copper electrode and flange assembly.

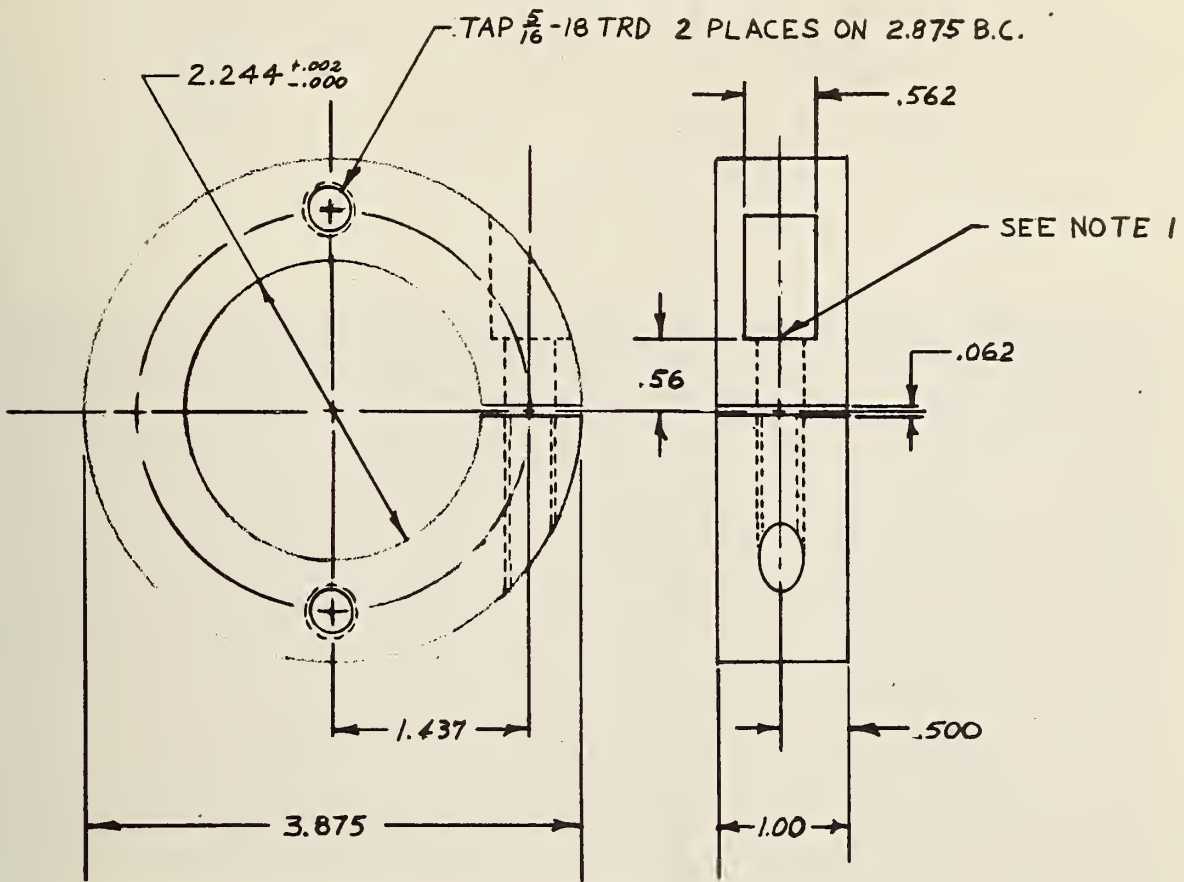Figure 6. Drawing of copper electrode supplying current to platinum electrode.

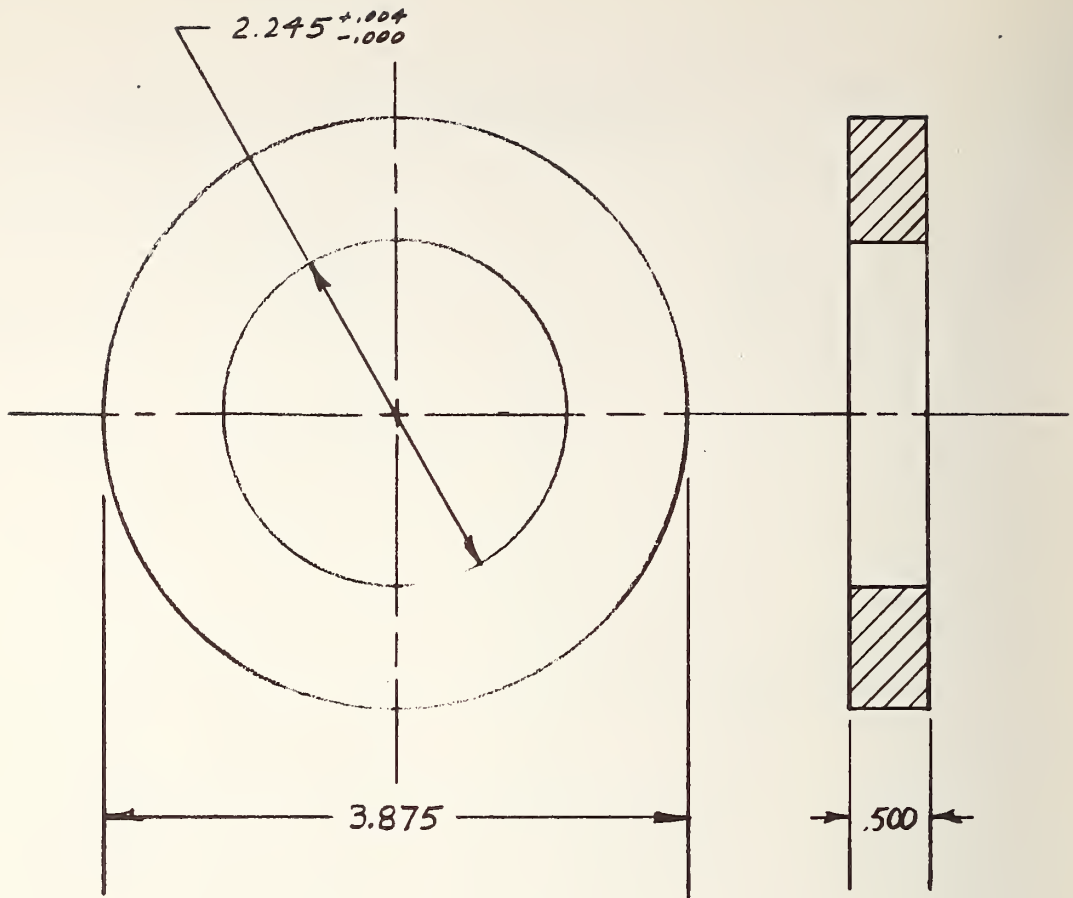Figure 7. Drawing of split lock collar for clamping copper electrode into flange.

Figure 8. Drawing of retaining ring used for clamping copper electrode into flange.
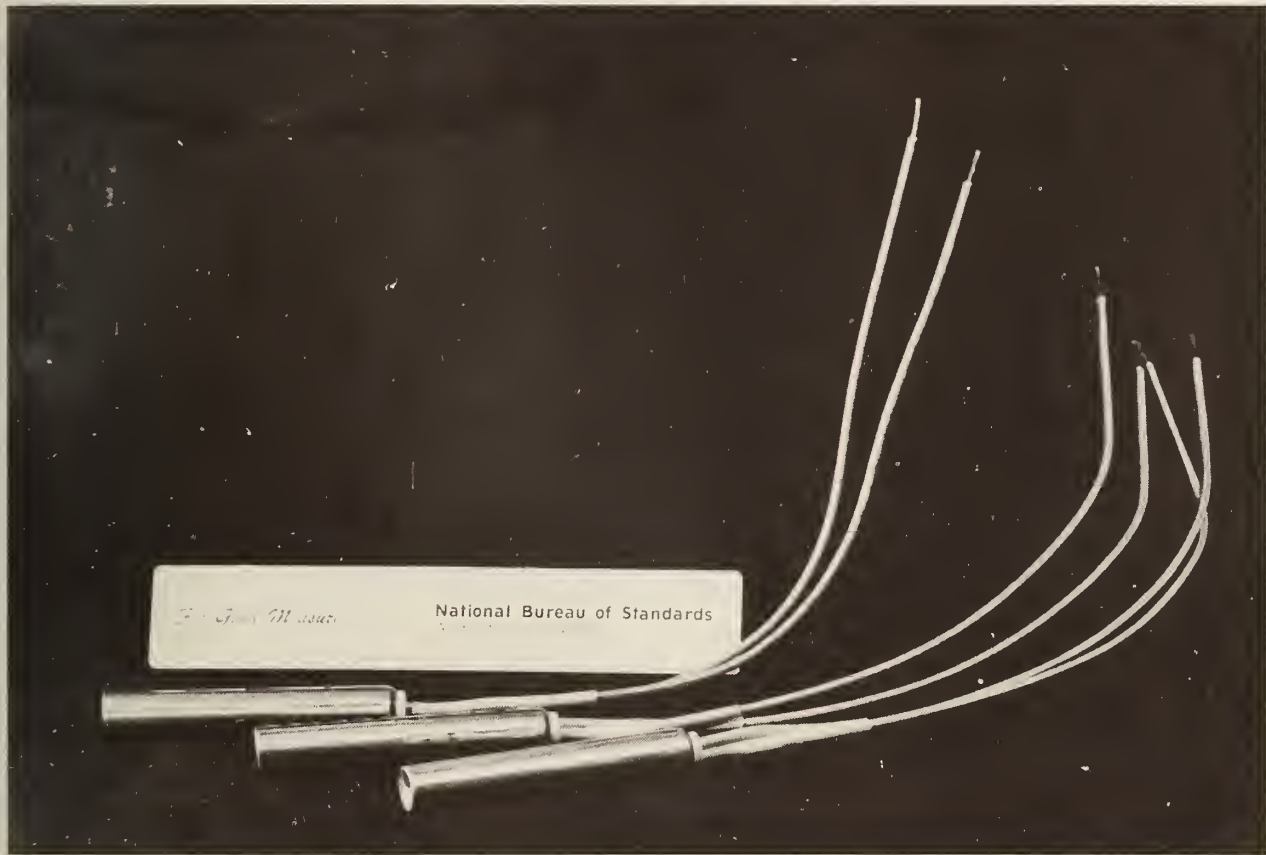
Figure 9. Bayonet heaters used for steam generator.

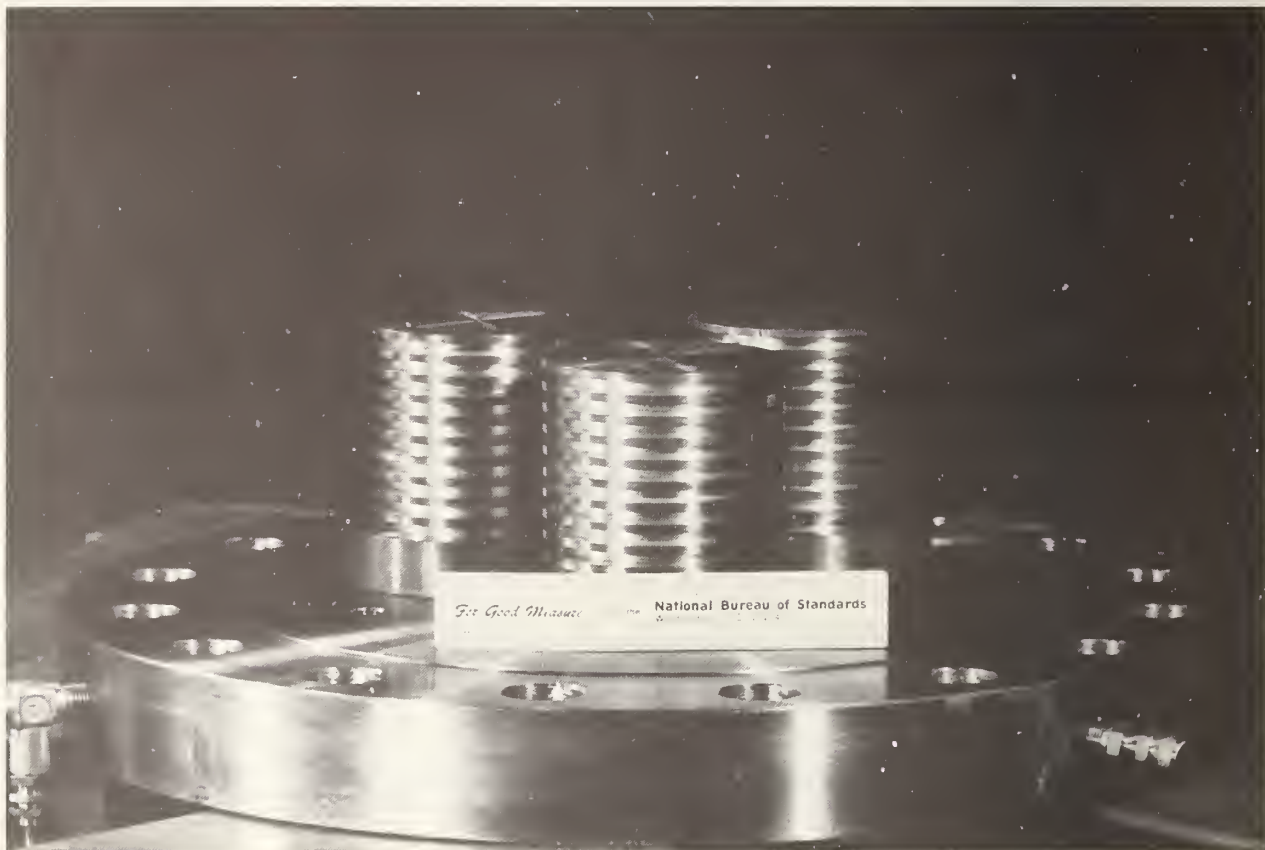Figure 10. Heat exchangers used to isolate bayonet heaters from pressure
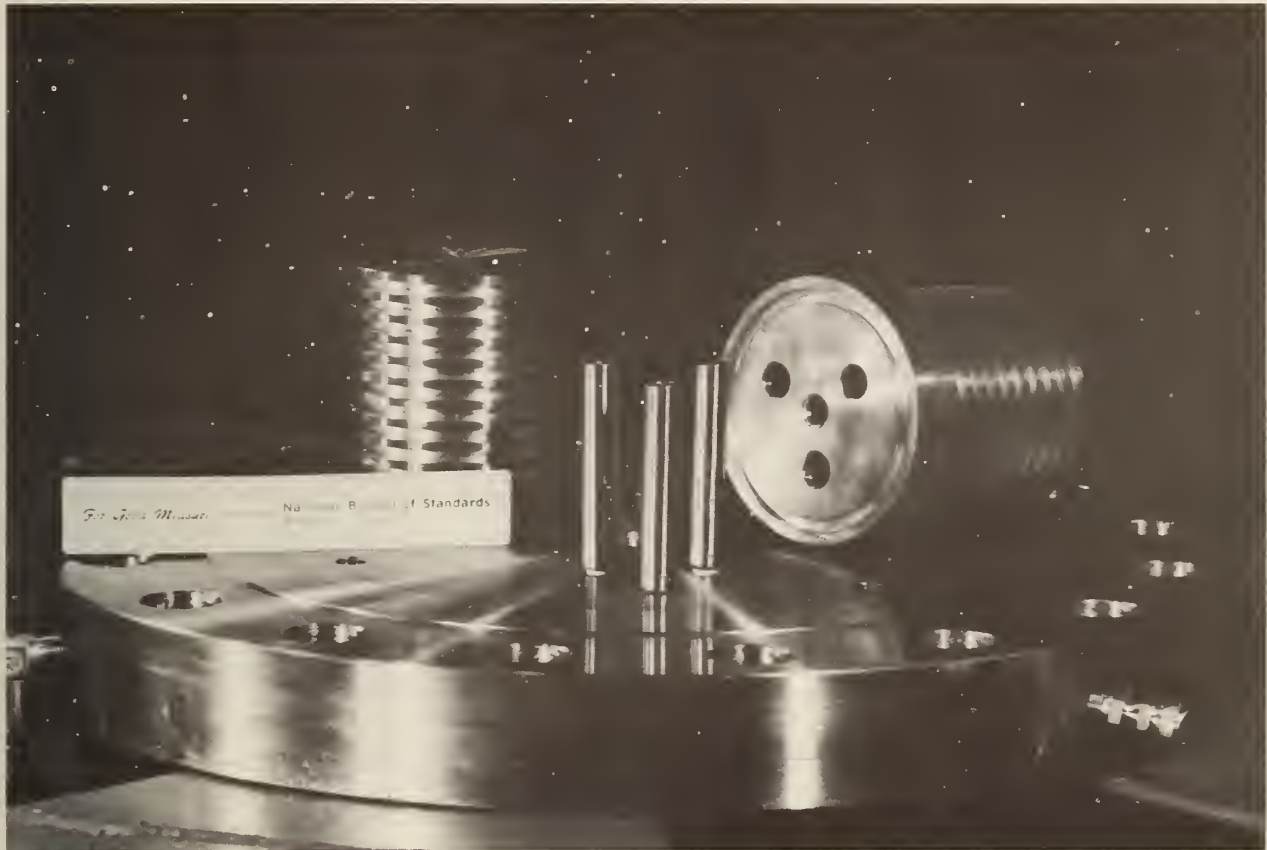and to transmit heat for steam generator.

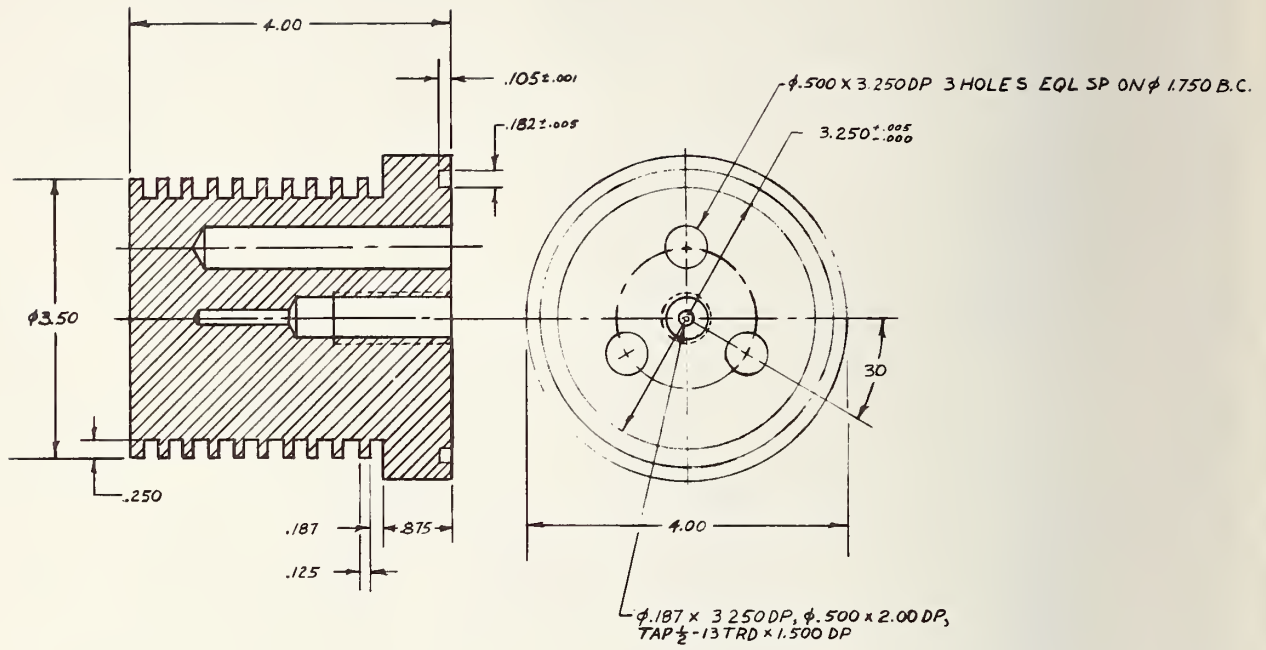Figure 11.   Heat exchangers and bayonet heaters.

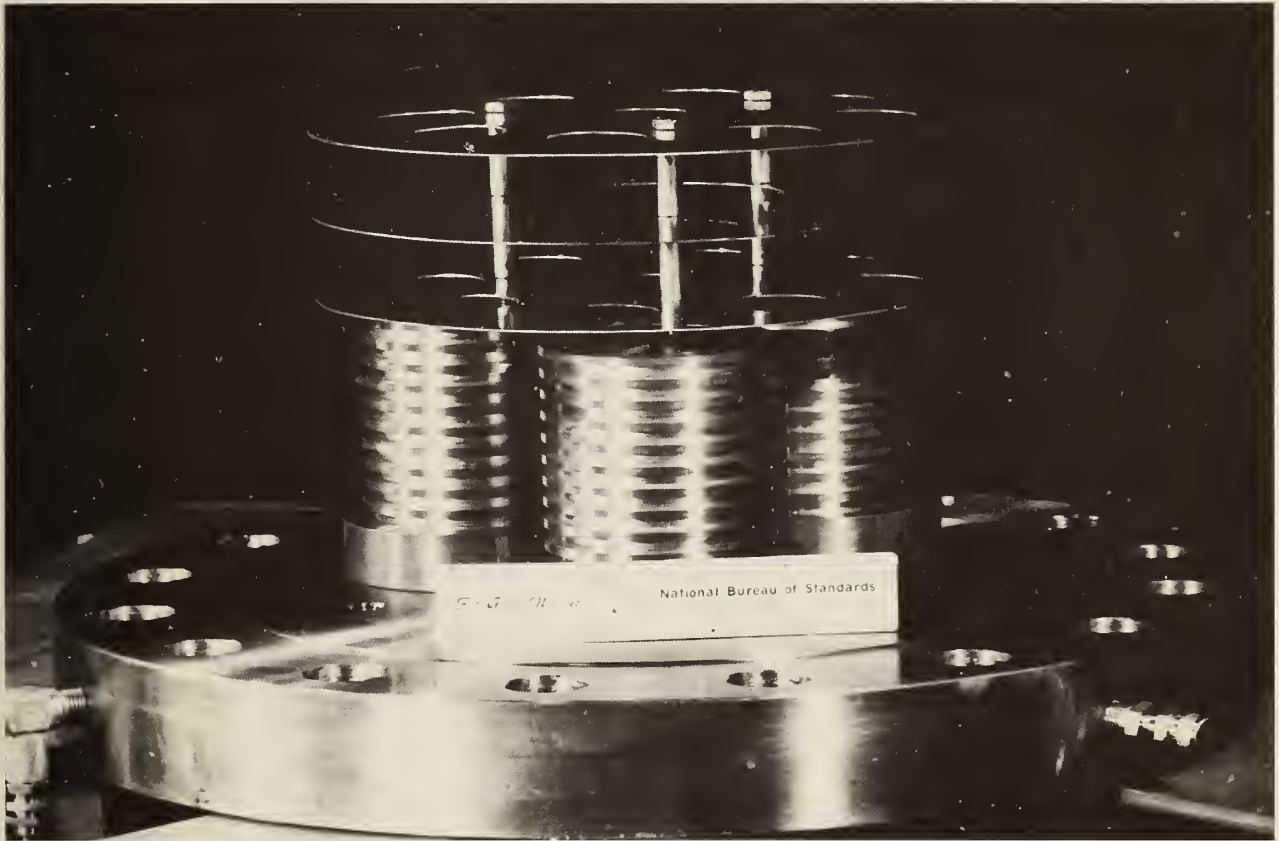Figure 12. Drawing of heat exchangers.

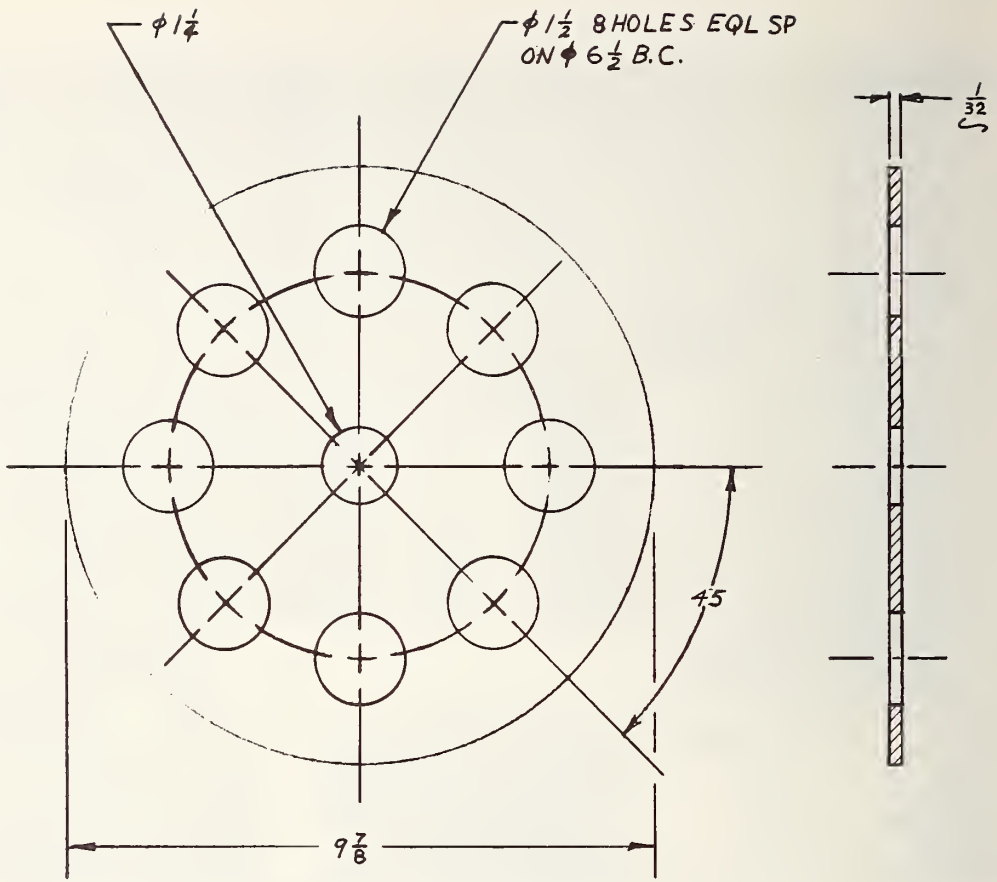Figure 13.   Heat exchangers and convection baffles.

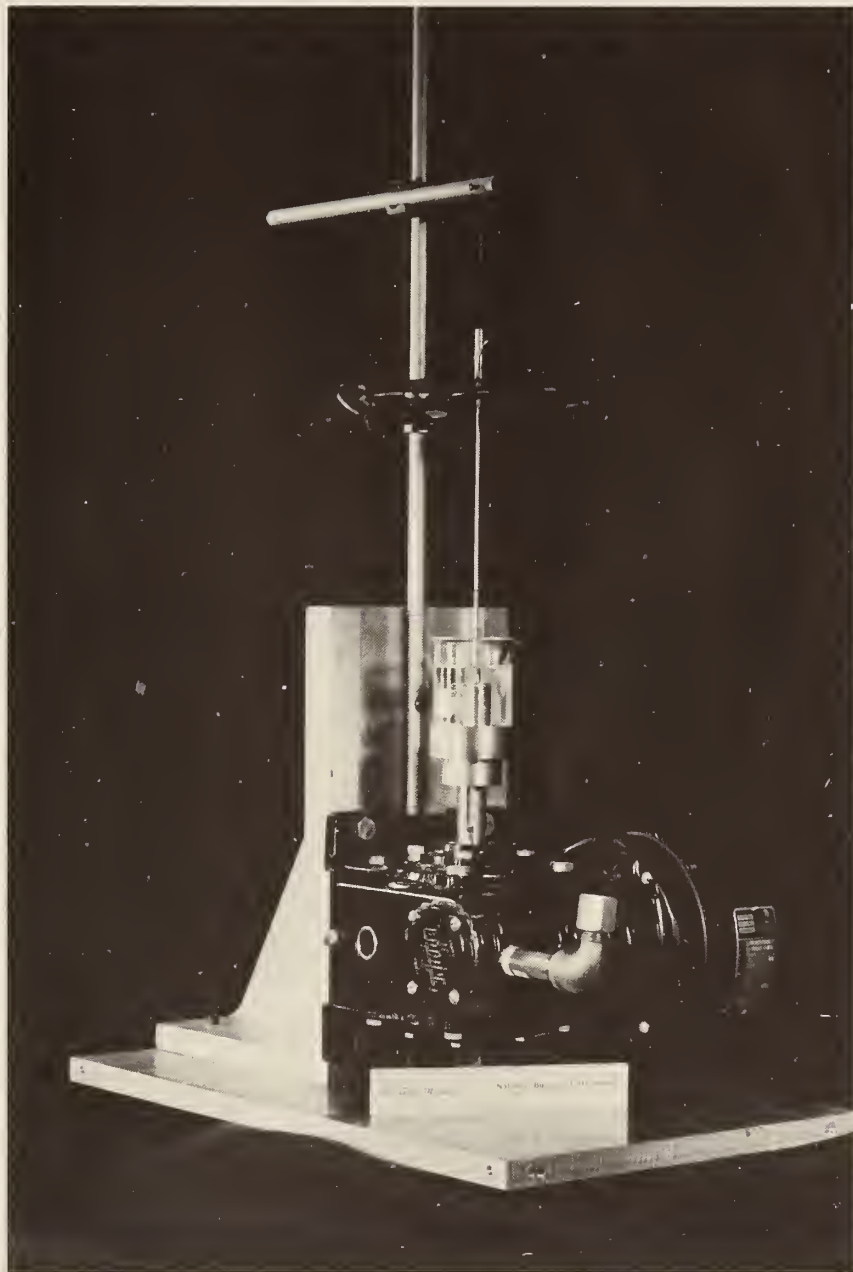Figure 14. Drawing of convection baffles.

Figure 15. Viscometer drive mechanism showing bob and
suspension similar to that employed in high
temperature pressure vessel.

c. Vaporization and Chemical Transport (J. Hastie and D. Bonnell, 313.01)

Progress: Using the redesigned reactor constructed during the second quarter (FY 77), we have carried out an extensive series of calibration tests using Na_2SO_4 and $NaCl$ as test materials. A schematic of this latest reactor design is shown in Figure 1 and an external photographic view of the reactor components is provided by Figure 2. Note in Figure 1 the close proximity of the sample boat, thermocouple and sampling orifice, thus ensuring an essentially isothermal condition between these three key elements of the reactor. During operation, the reactor is coupled to a molecular beam High Pressure Sampling Mass Spectrometer system which has been described in detail elsewhere*.

The vaporization results of our calibration tests have been analysed, using conventional second and third-law thermodynamic treatments, to indicate that the composition of the molecular beam generated by the reactor sampling probe is a good representation of the gas-vapor composition in equilibrium with the condensed phase (Na_2SO_4 or $NaCl$ in this case). Typical data obtained with this reactor are shown in the plots of Figures 3 and 4. Here the vapor composition data are summarized in the form of reaction equilibrium constants K_p for the reactions

$$Na_2SO_4 \text{ (solid or liquid)} = 2Na + SO_2 + O_2$$

and

$$NaCl \text{ (solid or liquid)} = NaCl$$
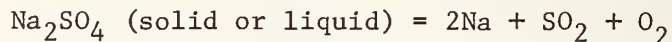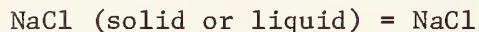
We should stress that these test salts are highly reactive materials in their liquid and vapor forms and the demonstrated good reactor performance in these cases leads to an optimistic outlook for the reactor capability under the planned simulated coal-gasifier conditions. Data such as those represented in Figures 3 and 4 are unique, as heretofore there has not existed a technique capable of monitoring the molecular weights and partial pressures of high temperature species in complex vapors at total pressures in the vicinity of 1 atm.

While we are confident that much useful data on coal gasifier reactions can be obtained with our present apparatus, we believe it important to pursue, eventually, the more difficult problem of making analogous measurements at much high pressures, $i.e.$, 20 atm or more. Such a prospect was envisioned in our original project proposal, and can now be initiated using supplementary funds from our related projects in flame chemistry. Accordingly, during this past quarter we have designed a new so-called Ultra High Pressure Sampling Mass Spectrometer system, details of which can be provided in a later report. The key improved performance factors designed into the new system are as follows:

● ability to sample from larger capacity reactors ($i.e.$, $\sim m^3$ vs $\sim cm^3$ gas volume)

50

● sampling from vertical, as opposed to the present horizontal, reactor orientations

● sampling of high temperature ($\sim$ 1400 C) gases and vapors at pressures of at least 20 atm, as compared with the present 1 atm limitation

● use of larger sampling orifices, *e.g.*, 20 mil as compared with the present use of 3 mil orifices--thus reducing any tendency for orifice plugging by small particles.

Each of these new performance factors should allow for a much closer approach to actual coal-gasifier conditions. This capability will be particularly important for those reactor conditions where large departures from thermodynamic equilibrium exists; though at present we do not have any specific information about what these conditions are likely to be. It should be noted that our present transpiration reactor is capable of operating at much higher pressures (*i.e.*, $\sim$ 10 atm) than the mass spectrometer system is capable of handling. Use of faster vacuum pumps and additional differentially pumped vacuum chambers, as has been designed into the new system, would allow for better utilization of the present reactor.

Plans: We expect to proceed with our original plan of systematically increasing the chemical complexity of the gas-solid (or liquid) reactions to be monitored with our present reactor--mass spectrometer system. Specifically, during the next quarter we will monitor the vapor transport processes for Na_2SO_4 and $NaCl$ in the presence of high partial pressures of SO_2, O_2 and H_2O.

* Hastie, J. W. Combustion and Flame, 21, 187 (1973).
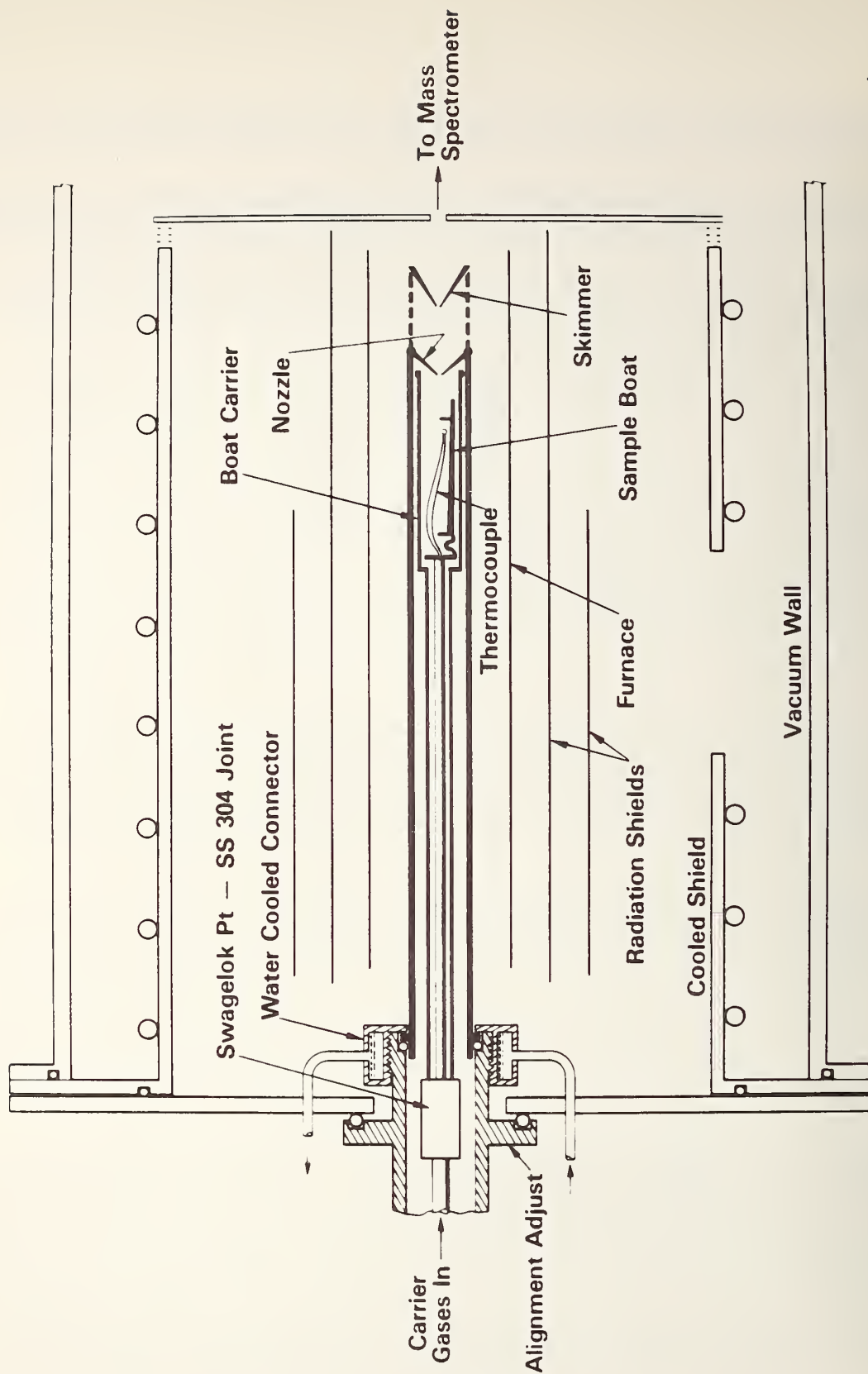
Figure 1. Schematic of Transpiration Reactor Assembly for generating a molecular beam representative of the gas-vapor composition.

Figure 2. Photo of main Transpiration Reactor components, showing the thermocouple, sample boat and Pt reactor with nozzle and skimmer attached.
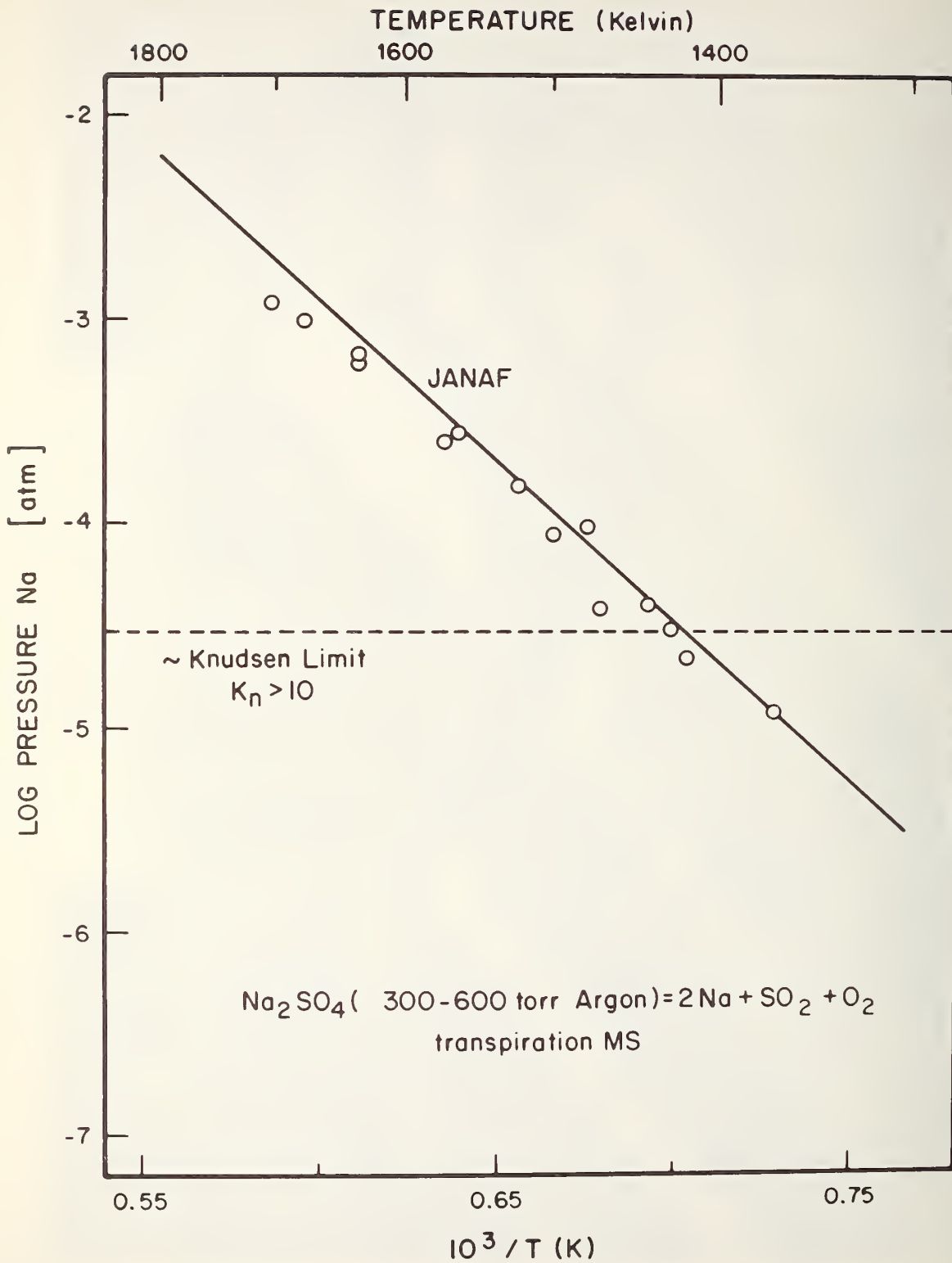
Figure 3. Variation of $Na_2SO_4(\ell)$ decomposition pressure with temperature, expressed in the second law thermodynamic form of log Na pressure vs. reciprocal temperature. Circled data points were obtained with the Transpiration Mass Spectrometer system. The solid curve is the literature data as summarized by the JANAF Thermochemical Tables—the experimental data were normalized using NaCl to calibrate the reactor.
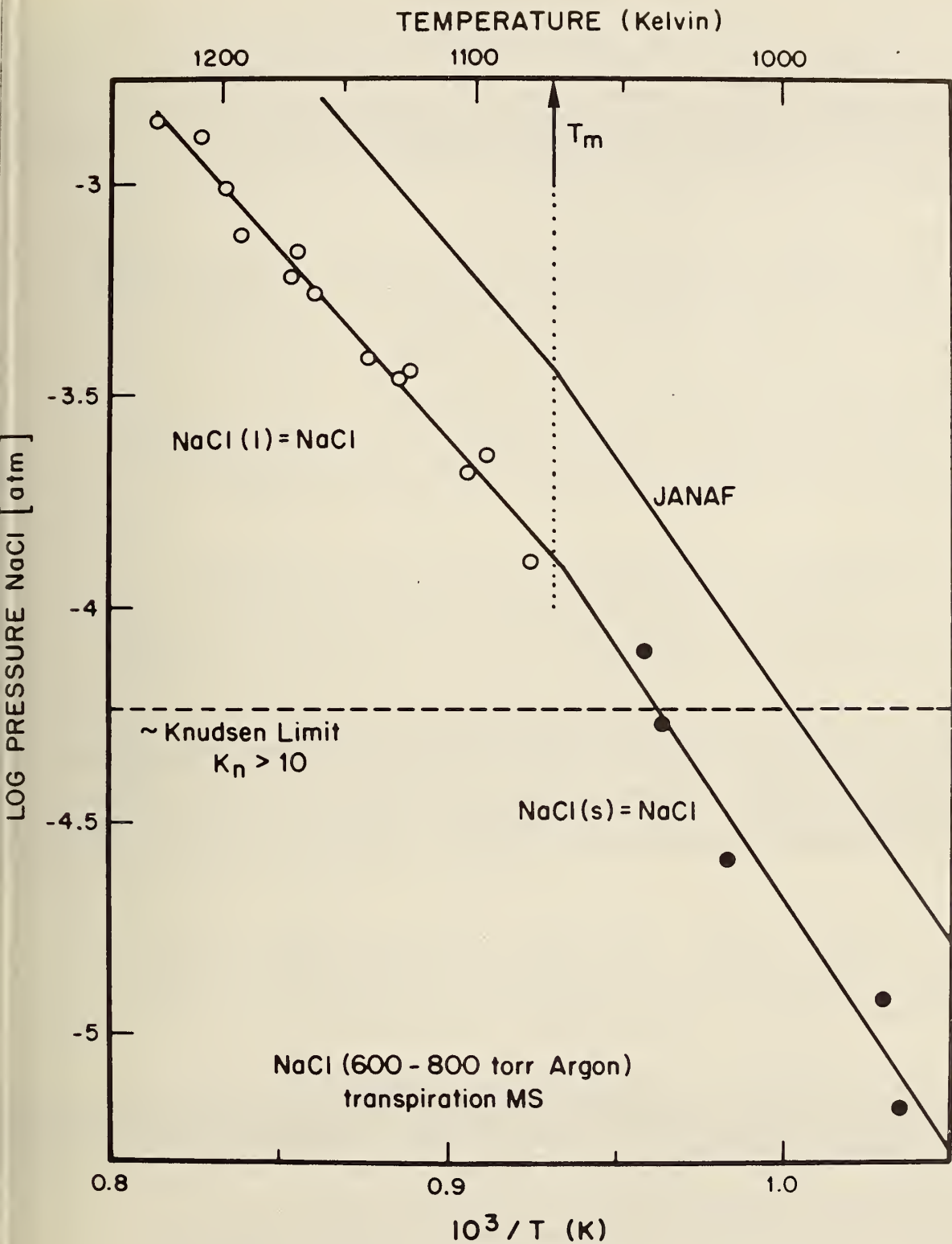
Figure 4. Variation of apparent NaCl vapor pressure with temperature using the argon mass spectrometric ion intensities to convert NaCl+ intensities to partial pressures. The observed displacement of the experimental and literature (i.e., JANAF) curves is attributed to the different free jet expansion properties of argon and NaCl and to their different ionization cross sections.

55

4. Failure Prevention (J. H. Smith, W. A. Willard and R. C. Dobbyn, 312.01)

<u>Progress</u>: During the quarter the Failure Prevention Information Center received fifty-eight reports of operational malfunctions and components and materials failures in coal conversion pilot plants and process development units. This number includes several diagnostic failure analyses from Oak Ridge National Laboratories and Argonne National Laboratories. To date, the percent contribution of information items coming from different coal conversion processes is shown in Table 1.

These reports have been classified and evaluated for technical completeness and accuracy and certain discrepancies have been resolved. Detailed abstracts of this information have been entered into the computerized data base management system. A recent update of the frequency of failure modes, which analyses all information in the system, is shown in Table 2.

The Information Center continued its close collaboration with Battelle - Columbus in the preparation of the ERDA Materials and Components Newsletter feature on failure experiences. Weekly updates of all abstracts are furnished to Battelle together with complete copies of all significant information.

During this quarter the Information Center handled forty-one separate requests for information. In response to these inquiries, copies of 827 abstracts, 67 complete reports and over 20 copies of the draft abstract reports were sent out. In addition, 10 visitors to the Center were briefed on its scope, operation and future plans.

Three additional abstract reports were prepared; each addresses a specific failure mode: erosion, corrosion and stress-corrosion cracking. This brings the total number of abstract reports to nine. The abstract report has been chosen as the initial format for the timely and efficient dissemination of information from the Center. Two of these reports, Corrosion and Incoloy 800, are in the final stages of NBS editorial review and should be available shortly.

Direct contact with pilot plant and failure analysis laboratory personnel was initiated during the quarter with visits to Synthane, MERC, BIGAS and the Westinghouse PDU completed. This activity has established firm channels of communication between the plants and the Center and has also provided additional failure and plant operation data.

Project staff also developed a detailed plan for a materials and components performance analysis of the CO_2 Acceptor Pilot Plant, including the establishment of a task force of ERDA, NBS and plant personnel. The study is to be conducted by ERDA later this year.

<u>Plans</u>: The information gathering phase of this project will continue as more information is received and additional contacts are made with pilot plants, process development units, failure analysis laboratories and other coal conversion technology centers. Additional abstract reports, now in various stages of completion, will be issued and new, more extensive, in-depth failure information dissemination schemes will be explored.

In addition to this expanded Information Center activity considerable effort is expected to be devoted to the review and evaluation of the performance of materials and components used in the CO_2 Acceptor Process pilot plant over the next eight months.

Table 1

COAL CONVERSION PROCESSES

NO. OF ITEMS	PERCENT	PROCESS
7	1.71	ALL
1	0.24	BIGAS
1	0.24	BIOMASS
16	3.92	BMI
10	2.45	CARBONATE
17	4.16	CLEAN COKE
1	0.24	COED
70	17.15	CO2
2	0.49	CPC
2	0.49	EXXON
1	0.24	GFERC
64	15.68	HYGAS
1	0.24	LERC
24	5.88	LIGNITE
15	3.67	MERC
29	7.10	MISC.
3	0.73	PERC
1	0.24	RANN
2	0.49	SEVERAL
31	7.59	SRC
2	0.49	SRC-W
89	21.81	SYNTHANE
4	0.98	SYNTHOIL
1	0.24	UNKNOWN
14	3.43	WESTINGHOUSE

408 = Total Number of Items in File.

58

Table 2

NUMBER OF REPORTED INCIDENTS OF FAILURES
IN COAL CONVERSION PLANTS

FAILURE MODE ANALYSIS

FAILURE MODE	CO$_2$ HYGAS	SRC	SYNTHANE	OTHER	TOTAL
CORROSION	48	32	11	24	58	173
AQUEOUS	0	2	0	0	3	5
CARBURIZATION	10	2	0	0	5	17
METAL DUSTING	4	0	0	0	2	6
OXIDATION	4	3	0	0	5	12
PITTING	3	5	3	5	9	25
SULFIDATION	16	11	0	7	3	37
GENERAL	11	9	8	12	31	71
STRESS-CORROSION	6	4	5	4	24	43
CHLORIDE	4	4	2	4	17	31
OTHER	2	0	3	0	7	12
MANUFACTURING DEFECT	14	9	13	18	34	88
DESIGN	6	3	13	8	25	55
FABRICATION	4	3	0	4	3	14
QUALITY CONTROL	4	3	0	6	6	19
EQUIPMENT MALFUNCTION	6	10	3	5	10	34
OVERHEAT	6	10	3	2	10	31
OVERSTRESS	0	0	0	3	0	3
EROSION	6	6	11	20	28	71
STRESS/TEMP FAILURE	1	6	1	6	14	28
CREEP	0	1	0	0	3	4
FATIQUE	0	2	0	3	9	14
THERMAL STRESS/SHOCK	1	3	1	3	2	10
UNKNOWN	2	11	0	19	7	39

NOTES

*   Incidents Reported to NBS Failure Prevention Information Center
    - Sponsored by ERDA, Fossil Energy
** Operating Times and Level of Reporting Vary with Each Plant

Appendix

5. Supportive Chemical Thermodynamics Calculations (W. S. Horton, 313.01)

Chemical thermodynamics calculations and computer programming were
begun this quarter in support of the materials testing under simulated
gasifier conditions. A need was recognized for having the capability
to perform calculations involving simultaneous chemical equilibria.
Consequently this short term activity was initiated.

It is very likely that the gaseous environment prepared for a test
will change composition; that it will change toward an equilibrium
composition if that is not the initial state. Although the extent
of the change will be limited by unknown chemical reaction rates,
it is important to know the maximum amount of change that can occur.
To provide this information requires calculations of simultaneous
chemical equilibria. This problem has been studied by many, and
specialized computer programs are available. However, it is necessary
to develop an interactive program that is useable with a timesharing
service. With such a program properly developed, the personnel perform-
ing tests may, with a few simple operations at a terminal, obtain answers
for any mixture of test gases they propose to use. This will be very
useful to such personnel particularly if they are not familiar with
details of chemical equilibria calculations and the complex batch computer
programs available for them.

The mathematics were reviewed, and the development was begun of an
algorithm based upon minimization of the Gibbs energy of the system.
Several tests of prototype programs have been made successfully.
These show that the algorithm works successfully when tailored to a
system of conditions and starting composition for which the existence
of condensed water and/or carbon is known *a priori*.

Plans: Efforts will be directed toward combining the simple cases
with respect to condensed species into a single general algorithm.
This problem together with that of convergence (or its equivalent:
initial estimates of equilibrium composition) are typically the
difficulties associated with writing computer programs for simultaneous
chemical equilibria.

TRANSPIRATION MASS SPECTROMETRY STUDIES OF THE THERMAL DECOMPOSITION AND SUBLIMATION OF SODIUM SULFATE

J. W. HASTIE, D. W. BONNELL AND D. M. SANDERS
Institute for Materials Research
National Bureau of Standards
Washington, D. C. 20234

Past experience in our laboratories using modulated beam mass spectrometry in Knudsen effusion and direct atmospheric sampling of flames has prompted an adaption of these techniques to the problems of sampling systems of interest under "real world conditions". Areas of interest here include sampling and characterization of model coal gasification environments and characterization of species involved in the vaporization of glasses.

Figure 1 shows a schematic of the high pressure sampler and an external photographic view of the components is provided by Figure 2. Certain features should be particularly noted. The entire high temperature region is platinum with minimal alumina exposure to minimize side reaction effects. The close proximity of sample boat, thermocouple, and sampling orifice (nozzle) ensure an essentially isothermal condition between these three key elements. The boat support minimizes dead volume and provides flow direction, a thermal equilibration baffle behind the boat, and good control of sample creep and vapor deposition. The water-cooled quick-connect assembly forms a high vacuum seal to the vacuum wall in an easily dismounted joint and allows easy cleaning of the entire sampler. During operation, the sampler is coupled to a molecular beam High Pressure Sampling Mass Spectrometer described in detail elsewhere (1) and the skimmed supersonic beam is carefully aligned to pass through the mass spectrometer ion source region with no collisions, preserving species present in the sampler essentially undisturbed.

The 2 cm spacing between nozzle and skimmer place the skimmer well inside the first Mach disk. Calculations using

$$Z_n \sim 2/3D(P_0/P_1)^{1/2} \sim 0.17(S_1)^{1/2} \text{ cm}$$

gives a nozzle to Mach disk distance Z_n of $\sim 3.6 \pm 0.5$ cm for a nozzle diameter D of 0.006 cm, a pressure ratio across the nozzle (region 0 is sample, region 1 is vacuum) $P_0/P_1 \cong 10^6$, or an effective region 1 pumping speed $S_1 \cong 500$ ℓ/sec net.

With argon gas as a carrier in the transpiration mass spectrometer sampler, a measurement of phase shift compared to that for molecular effusion allowed calculation of beam velocity. The beam velocities observed during experimental runs were within 10% of the theoretical supersonic beam velocity indicating good adherance to supersonic sampling technique. No argon clusters were observed, but both the very small nozzle orifice diameter and high expansion rate used here minimize such clustering.

Calibration and test runs using NaCl were made to check operation of the sampler. The reaction equilibrium constant K_p for the reaction

NaCl(liquid) = NaCl(gas)
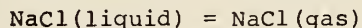
was determined as log K_p(atm) = 4.44-8927/T. A derived second law heat of vaporization of 41±2 kcal/mole is in good agreement with the JANAF (2) value of 43.7 kcal/mole. This generally excellent agreement in second law ΔH_{vap} with the JANAF tabulation confirms the conclusion that the composition of the beam generated by the sampling system is a good representation of the gas-vapor composition in equilibrium with the condensed phase.

The vapor decomposition data for the reaction

$$Na_2SO_4(liquid) = 2Na + SO_2 + O_2$$

expressed as P(Na) are shown in Figure 3. The data are in quite reasonable agreement with the JANAF compilation (solid curve in Figure 3) and the Knudsen data of Kohl, Sterns, and Fryburg (3) and Ficalora, et al. (4).

An ion signal corresponding to the Na_2SO_4 molecule was just detected at the upper end of our temperature range with an intensity approximately 1% of that predicted by comparison with Knudsen data of Kohl, *et al*. (3). A possible explanation may lie in observations by Gurvich (5) in his observations of K_2SO_4 where a temperature dependent fragmentation effect was noted.

REFERENCES

1. Hastie, J. W., Combustion and Flame 21, 187 (1973).

2. JANAF Thermochemical Tables, 2nd Ed., NSRDS-NBS-37 (1971).

3. Kohl, F. J., Stearns, C. A., Fryburg, G. C., NASA TM X-71641 (1975).

4. Ficalora, P. J., Uy, O. M., Muenow, D. W., and Margrave, J. L., J. Amer. Ceram. Soc. 51, 574 (1969).

5. Gurvich, L. V., Proceedings of the High Temperature Sciences Related to Open-Cycle, Coal-Fired MHD Systems Conference held at Argonne National Laboratories on April 3-6, 1977, in press.
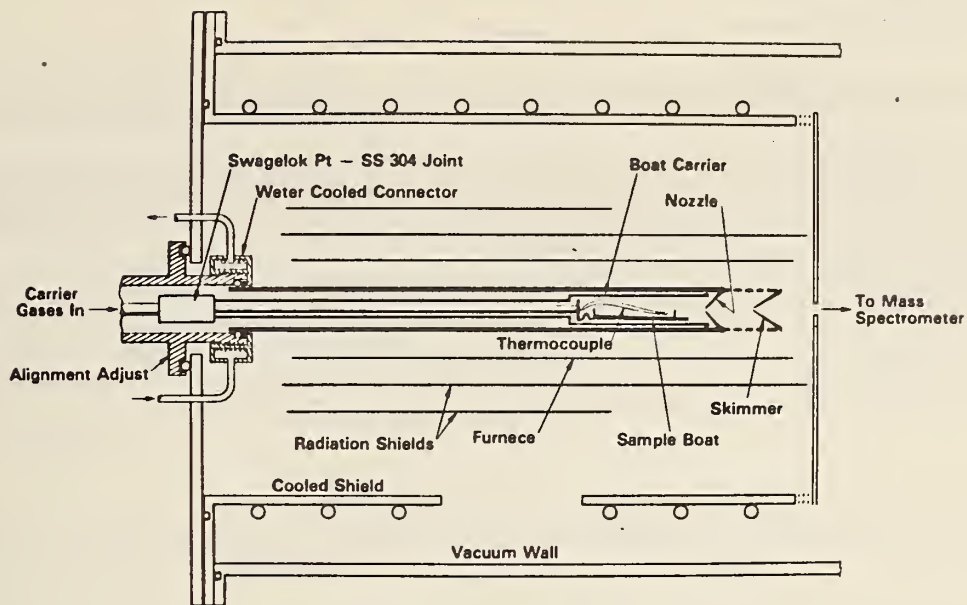
FIGURE 1.
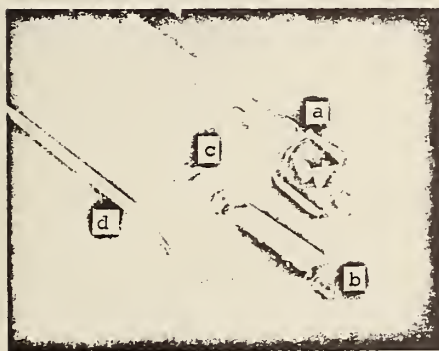SCHEMATIC OF TRANSPIRATION MASS SPECTROMETER
INLET SYSTEM

FIGURE 2.
PHOTOGRAPH OF SAMPLER COMPONENTS
a. Platinium sampler with nozzle
   and attached skimmer
b. Boat.
c. Boat carrier.
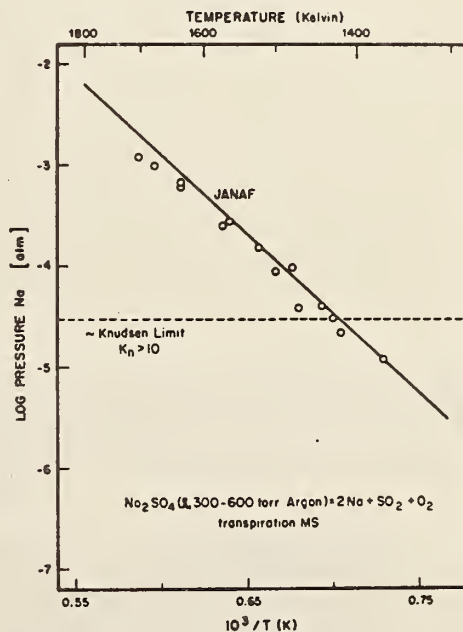d. Thermocouple in Al_2O_3 insulator

FIGURE 3.
Na_2SO_4 DECOMPOSITION REACTION
● observed P(Na)
solid line- JANAF tabulation

OGRAPHIC DATA SHEET	FE-3800-12		No.		

TLE AND SUBTITLE	5. Publication Date
"MATERIALS RESEARCH FOR CLEAN UTILIZATION OF COAL" Quarterly Progress Report, April 1 - June 30, 1977	July 1977
	6. Performing Organization Code
	N8SIR 77-1296

7. AUTHOR(S) Samuel J. Schneider, Jr.	8. Performing Organ. Report No.

9. PERFORMING ORGANIZATION NAME AND ADDRESS	10. Project/Task/Work Unit No.
NATIONAL BUREAU OF STANDARDS DEPARTMENT OF COMMERCE WASHINGTON, D.C. 20234	11. Contract/Grant No.
	E(49-1)-3800

12. Sponsoring Organization Name and Complete Address (Street, City, State, ZIP)	13. Type of Report & Period Covered Quarterly Progress Report
Energy Research and Development Administration 20 Massachusetts Avenue, N.W. Washington, D. C. 20545	14. Sponsoring Agency Code
	Dist. Cat. UC-90C

15. SUPPLEMENTARY NOTES

16. ABSTRACT *(A 200-word or less factual summary of most significant information. If document includes a significant bibliography or literature survey, mention it here.)*

This progress report covers work on metal corrosion, metal erosion, ceramic deformation, fracture, erosion, and chemical degradation as related to coal gasification systems. This report also covers the failure avoidance program for ERDA coal conversion pilot plants.

17. KEY WORDS *(six to twelve entries; alphabetical order; capitalize only the first letter of the first key word unless a proper name; separated by semicolons)* Ceramic corrosion, ceramic erosion, ceramic fracture, chemical degradation, coal gasification material, failure avoidance, metal corrosion, metal erosion, and vaporization processes

18. AVAILABILITY ☐ Unlimited	19. SECURITY CLASS (THIS REPORT)	21. NO. OF PAGE
☒ For Official Distribution. Do Not Release to NTIS NBS will not submit to NTIS; ERDA-FE will submit after approval.	UNCLASSIFIED	
☐ Order From Sup. of Doc., U.S. Government Printing Office Washington, D.C. 20402, SD Cat. No. C13	20. SECURITY CLASS (THIS PAGE)	22. Price
☐ Order From National Technical Information Service (NTIS) Springfield, Virginia 22151	UNCLASSIFIED	

USCOMM-DC 29042-

6434